Analytical Performance Evaluation of STAR-RIS Assisted Terahertz Wireless Communications

DOI:
10.1109/TVT.2023.3336260

Document Version
Accepted author manuscript

Citation for published version (APA):
Khel, A. M. T., & Hamdi, K. A. (2023). Analytical Performance Evaluation of STAR-RIS Assisted Terahertz Wireless Communications. *IEEE Transactions on Vehicular Technology*. https://doi.org/10.1109/TVT.2023.3336260

Published in:
IEEE Transactions on Vehicular Technology

Analytical Performance Evaluation of STAR-RIS Assisted Terahertz Wireless Communications

Ahmad Massud Tota Khel, and Khairi Ashour Hamdi, *Senior Member, IEEE*

***Abstract*—This paper considers simultaneous transmitting and reflecting reconfigurable intelligent surface (STAR-RIS) assisted terahertz communications, in which a multi-antenna full-duplex base station serves two half-duplex users (U1 and U2) in the downlink and uplink, respectively. It is assumed that U1 and U2 are located in the reflection and transmission spaces. The STAR-RIS is considered under energy splitting (ES) and mode switching (MS) protocols to provide simultaneous full-space coverage to both users, but at the expense of inter-user interference (IUI). The paper aims to evaluate the impacts of various practical factors on the system performance, including IUI, quantization errors due to discrete phase shifters of the STAR-RIS, beam misalignment due to highly-directive antennas, and random fog. Thus, it derives accurate expressions for the ergodic capacity, outage probability, and symbol error rate. Numerical and simulation results reveal that the system performance is more severely impacted by beam misalignment and random fog than by other factors. It is also observed that the ES protocol outperforms the MS protocol in the downlink, but the situation is reversed in the uplink due to coupled phase shifts. Moreover, in the high-signal-to-noise ratio regime, the system performance is restricted due to IUI signals.**

***Index Terms*—Beam misalignment, interference, phase errors, random fog, reconfigurable intelligent surfaces, terahertz.**

I. Introduction

FUTURE sixth-generation (6G) wireless networks are anticipated to exceed 1 terabit per second, revolutionizing communication for advanced technologies like virtual reality, holographic communication, and autonomous vehicles [1], [2]. The terahertz (THz) band, spanning from 0.1 THz to 10 THz, holds promise for achieving the ultra-high data rate requirements of 6G [3]. To meet the ever-growing data rate demands, it is crucial to not only expand the transmission bandwidth, but also improve the spectral efficiency [2]. Therefore, by exploiting the full-duplex (FD) technology which allows two or more users to simultaneously communicate over the same bandwidth, the spectral efficiency is remarkably improved [4]. Although the FD process introduces self-interference (SI), which is a major limiting factor if left unresolved, it can be significantly mitigated by employing various SI cancellation (SIC) techniques, such as increasing the separation distance of transmit-receive antennas of an FD node, employing antenna diversity with beamforming, utilizing digital SIC methods, and intelligently modifying the propagation environment [4]–[8].

Manuscript received xx, 2023; revised xx, 2023; accepted xx, 2023. Date of publication xx, 2023; date of current version xx, 2023. *(Corresponding author: Ahmad Massud Tota Khel.)*

The authors are with the Department of Electrical and Electronic Engineering, The University of Manchester, Manchester M13 9PL, United Kingdom (e-mail: ahmadmassud.totakhel@postgrad.manchester.ac.uk; k.hamdi@manchester.ac.uk).

Despite offering ultra-high data rates, THz communications are highly vulnerable to obstructions and environmental factors. For instance, the presence of molecules and small particles, e.g. water vapor and oxygen, in the atmosphere results in the absorption of THz signals' energy [9]–[12]. Moreover, the narrow beamwidth THz waves are prone to beam misalignment caused by thermal expansions, building sways, and dynamic wind loads, leading to significant signal attenuation [9], [12], [13]. Furthermore, random foggy weather conditions also result in substantial attenuation of THz signal power [14]–[18]. Therefore, it is essential to effectively mitigate these challenges to improve the reliability of THz systems. As such, among various technologies, deploying a vast array of antennas is a potential solution; however, the deployment of numerous active components leads to increased hardware and signal processing complexity, energy consumption, and cost [1], [19].

Reconfigurable intelligent surfaces (RISs) are a promising solution composed of a low-cost and passive array of elements, allowing for the smart manipulation of the propagation environment and directing incident signals to desired destinations [1], [20], [21]. Although a reflecting-only RIS improves the performance of wireless systems, its effectiveness is limited due to its reliance on users and base stations (BSs) being within the RIS's reflection space. In contrast, a simultaneous transmitting and reflecting RIS (STAR-RIS) is a two-sided transparent surface that can simultaneously reflect and transmit signals by providing indirect paths to users and BSs located on both sides (reflection and transmission spaces) [19], [22]. Moreover, several studies have shown that by intelligently designing the phase shifts of RISs, it is possible to combine the reflected/transmitted signals constructively at the desired destination and destructively at the undesired destination, which leads to simultaneous performance improvement and effective interference mitigation [23]–[25]. In particular, when accounting for the effects of distance-dependent path-loss, RISs can substantially mitigate the inter-cell interference (ICI).

The authors of [19] have proposed three protocols for the operation of STAR-RISs: time switching protocol, where the elements at each instance of time can either reflect or transmit the incident signals; mode switching (MS) protocol, where the elements are divided into two groups, each one for reflection and transmission only; and the energy splitting (ES) protocol, where each element simultaneously reflects and transmits the incident signals. Moreover, the authors in [30]–[32] have shown that a STAR-RIS can support dual-sided simultaneous reflection and transmission. This capability allows a STAR-RIS to reflect and transmit signals incident on both sides, making it a promising solution for simultaneous uplink and downlink communication [22], [26]–[29], [33], [34].

TABLE I Summary of Existing Literature

Ref.	THz	STAR-RIS	Reflecting-only RIS	Phase Error	Beam Misalignment	Random Fog	Interference	Metric
[5]	✗	✗	✓	✗	✗	✗	✓	EC, SER
[6]	✗	✗	✓	✗	✗	✗	✓	BLER
[7]	✗	✗	✓	✓	✗	✗	✗	OP
[8]	✗	✗	✓	✗	✗	✗	✓	EC, OP, BLER
[9]	✓	✗	✓	✗	✓	✗	✗	EC, OP
[10]	✓	✗	✓	✗	✓	✗	✗	SER
[11]	✓	✗	✓	✗	✗	✗	✓	Sum rate
[12]	✓	✗	✗	—	✓	✗	✗	EC, OP
[13]	✓	✗	✓	✓	✓	✗	✗	EC
[15]	✓	✗	✗	—	✗	✓	✗	SER
[16]	✓	✗	✗	—	✓	✓	✗	EC, OP, SER
[17]	✓	✗	✗	—	✓	✓	✗	EC, OP
[18]	✓	✗	✗	—	✓	✓	✗	OP, SER
[20]	✓	✗	✓	✗	✓	✗	✗	EC, OP, SER
[21]	✓	✗	✓	✗	✓	✗	✗	OP
[22]	✗	✓	✓*	✗	✗	✗	✓	Sum rate
[26]	✗	✓	✓*	✗	✗	✗	✓	Sum rate
[27]	✗	✓	✓*	✗	✗	✗	✓	EC
[28]	✗	✓	✓*	✗	✗	✗	✓	Sum rate
[29]	✗	✓	✓*	✗	✗	✗	✓	Sum rate
This work	✓	✓	✓*	✓	✓	✓	✓	EC, OP, SER

✓: considered, ✓* : compared with conventional reflecting-only RIS or HD, ✗ : not considered, — : not applicable, EC : ergodic capacity, OP : outage probability, BLER : block length error rate, and SER : symbol error rate.

A. Prior Works

As shown in TABLE I, a number of studies on the analytical performance evaluation of conventional reflecting-only RIS-assisted half-duplex (HD) THz communications have been reported (e.g. [9], [10], [13], [20], [21]). In more details, the authors in [9] have analyzed the capacity and outage performance of a reflecting-only RIS-assisted THz system in the presence of beam misalignment. However, the presented analytical expressions are based on the assumption of optimal phase shifts, and upper-bounded channel gain. In [10], the symbol error rate (SER) of reflecting-only RIS-assisted THz satellite communications in the presence of beam misalignment under the assumption of optimal RIS phase shifts has been studied. The authors in [13] have assessed the secrecy capacity of a reflecting-only RIS-assisted THz system in the presence of beam misalignment and phase shift quantization errors. The SER, outage probability and ergodic capacity of a reflecting-only RIS-assisted THz system in the presence of beam misalignment under the assumption of optimal phase shifts have been studied in [20]. Moreover, the authors in [21] have considered reflecting-only RIS-assisted THz systems in the presence of beam misalignment under ideal phase shifts, where they have statistically characterized the RIS channels and analyzed the outage probability in different scenarios.

Several works on the beamforming design, transmit power minimization and rate maximization of STAR-RIS assisted conventional wireless systems have been reported (e.g. [22], [26]–[29], [35], [36]). The authors in [22] and [26] have considered a STAR-RIS assisted conventional FD system in the presence of interference between HD uplink and downlink users, where they have optimized the reflection coefficients to maximize the sum rate. In [27], by considering interference from an uplink user, a new algorithm for beamforming design and power minimization of a STAR-RIS assisted conventional FD system has been proposed, where its superiority has been verified by comparing the performance of STAR-RISs and conventional RISs. The authors in [28] and [29] have performed beamforming design and optimized the amplitude coefficients, phase shifts, and transmit power to maximize the weighted sum rate of a STAR-RIS assisted conventional FD communication system in the presence of interference.

The authors in [35] have considered a STAR-RIS assisted conventional wireless system, where by considering the coupled reflection and transmission phase shifts, they have presented new optimization and deep reinforcement learning-based algorithms for the joint active and passive beamforming to minimize the power consumption. Furthermore, in [36], a STAR-RIS assisted conventional non-orthogonal multiple access communication system in the presence of coupled phase shifts has been considered. To improve the quality of service for the user located in the reflection space, a new joint power and discrete amplitude allocation scheme has been presented, and then the outage performance has been evaluated.

B. Motivations and Contributions

As discussed above and shown in TABLE I, the vast majority of the studies on the analytical performance evaluation of reflecting-only RIS assisted THz systems are based on the assumption of optimal phase shifts. Whereas, in practice, due to inherent constraints of the RIS hardware, it is unrealistic and not feasible. In fact, practical RISs are equipped with discrete phase shifters, where they can only apply discrete quantized phase shifts, and thus the incident signals are reflected/transmitted with phase shift quantization errors [36]–[38]. Moreover, in practical STAR-RISs, the phase shifts applied by the reflecting and transmitting elements are coupled to each other, which has been ignored in the vast majority of the aforementioned studies. Furthermore, none of the previously mentioned literature has examined the effects of random fog on the performance of RIS-assisted THz systems. Therefore, given the vulnerability of THz waves, it is necessary to analyze the impacts of various foggy weather conditions. In addition, taking into account the practical factors of THz, the impacts of interference on the performance of THz communications have not been investigated. To the best of our knowledge, in the existing literature, no work on the analytical performance evaluation of STAR-RIS assisted THz communications has been reported, specifically in the presence of beam misalignment, phase shift quantization errors, interference, and random fog.

Motivated by these considerations, we aim to evaluate the combined effects of beam misalignment and various random foggy conditions on the performance of STAR-RIS assisted THz systems under different STAR-RIS operation protocols. Moreover, we aim to investigate the advantages of employing a STAR-RIS to mitigate the limitations of THz communications. We also intend to evaluate the effects of phase shift quantization errors and interference signals transmitted/reflected by STAR-RISs. Therefore, the main contributions and findings of this paper can be described as follows.

- This paper focuses on the central cell of a multi-cell THz wireless network, consisting of a STAR-RIS and multi-antenna FD BS, simultaneously serving two HD users in the uplink and downlink. The STAR-RIS is examined under two protocols: (i) the ES protocol, and (ii) the MS protocol, where the users are assumed to be in the same cell and in close proximity to the STAR-RIS, and thus the uplink user causes considerable intra-cell or inter-user interference (IUI), affecting the downlink user's performance. Therefore, to evaluate the effects of IUI and practical factors of THz communications, it primarily focuses on evaluating the downlink user's performance.
- Deriving the exact probability density functions (PDFs) for the power of both the desired and interference signals is extremely difficult and almost intractable due to the involvement of a large number of random variables (RVs). Therefore, this paper approximates their PDFs using the Laguerre expansion, and the accuracy of the approximated PDFs for different numbers of STAR-RIS elements is verified by numerical and computer simulation results.
- It derives analytical expressions for the ergodic capacity, outage probability, and SER in terms of the characteristic functions (CHFs) and moment generating functions (MGFs) of desired and interference signals. Moreover, for deeper performance insights, it analyzes these metrics in the high-signal-to-noise ratio (high-SNR) regime.
- Although for brevity, this paper evaluates the impacts of IUI along with the practical factors of THz on the downlink user's performance, a subsection is provided to demonstrate that the analytical expressions can also be used to assess the performance of the FD BS in the uplink scenario with imperfect SIC and coupled phase shifts.
- In practical THz systems, the ICI signals are extremely weak and negligible due to several factors, such as phase shifts and severe path attenuation associated with relatively large inter-cell distances, obstacles, energy absorption, beam misalignment, and random fog [3], [23]–[25], [39]. Nonetheless, it is demonstrated that the analytical expressions are also applicable to cases in which the STAR-RIS reflects and/or transmits the ICI signals caused by multiple users and BSs located in neighboring cells.

Numerical and computer simulation results highlight the superiority of the ES protocol over the MS protocol in the downlink scenario, as the latter decreases not only the number of STAR-RIS elements randomly transmitting the IUI signals but also the elements reflecting the beamformed desired signals. However, in the uplink scenario, the MS protocol outperforms the ES protocol, since the latter is affected by selection errors associated with coupled downlink and uplink phase shifts. The results reveal that beam misalignment and random fog significantly degrade the system performance, more severely than IUI and phase shift quantization errors. It is also shown that achieving a normalized beamwidth of less than or equal to 0.5 (indicating very narrow beamwidth THz waves) can significantly improve the performance, making it almost identical to the performance achieved with perfectly aligned antennas. Therefore, attentive calibration of both transmit and receive antennas along with the STAR-RIS is crucial for reliable and effective THz communications. Moreover, it is observed that the adverse effects of random foggy weather and beam misalignment are mitigated by increasing the number of antennas and STAR-RIS elements.

It is observed that the system performance under non-optimal phase shifts is remarkably inferior to that achieved under optimal phase shifts. However, this effect can be greatly mitigated by increasing the quantization levels, albeit at the price of hardware complexity and cost. Moreover, the system performance reaches a limit in the high-SNR regime due to IUI signals, which remains unaffected by SNR enhancement but can be scaled by factors such as number of antennas, STAR-RIS elements, quantization levels, protocols, and amplitude coefficients. The effects of ICI signals arising from adjacent cells' users and BSs are also assessed, and they are found to be extremely minimal and negligible due to relatively large inter-cell distances, STAR-RIS phase shifts, and limiting factors of THz. It is also shown that the effects of IUI are alleviated by increasing the reflection amplitude coefficients of the STAR-RIS elements. Nonetheless, this along with the selection errors due to coupled phase shifts deteriorates the performance of uplink communication. Thus, it raises an optimization problem of improving users' performance while suppressing interference, which exceeds the scope of this paper.

Finally, it is observed that under both ES and MS protocols, the total capacity of the STAR-RIS assisted FD system significantly surpasses that of the reflecting-only RIS-assisted HD system, albeit at the expense of higher outage probability and SER. However, increasing the STAR-RIS phase shift quantization levels improves the outage probability and SER, outperforming the HD system in the relatively low-SNR regime, yet constrained by IUI signals in the high-SNR regime.

C. Organization and Notations

The system model and channels characterization are presented in Section II. Section III presents the statistical distributions of both the desired and interference signals' power, and the analytical expressions for the ergodic capacity, outage probability and SER. Section IV and Section V present the results and conclusion of the paper, respectively. In addition, the mathematical notations are illustrated in TABLE II.

TABLE II Mathematical Notations

Notation	Description	Notation	Description
$\lvert . \rvert$	absolute value	$\lvert\lvert . \rvert\rvert$	Frobenius norm
x^H	Hermitian transpose	$\mathrm{diag}\,(.)$	diagonal matrix
$\mathrm{Re}\,\{x\}$	real part of x	$\mathrm{Im}\,\{x\}$	imaginary part of x
$\mathbb{E}[x]$	expectation of x	$\mathrm{P_r}(x)$	probability of x
$\mathbb{E}[x\lvert y]$	expectation of x conditioned on y	$\mathrm{P_r}(x\lvert y)$	probability of x conditioned on y
$\mathbb{V}[x]$	variance of x	$f_x(x)$	PDF of x
$\Phi_x\,(\omega)$	CHF of x	$\mathcal{M}_x(-s)$	MGF of x

Notation	Description
$x \sim \mathcal{CN}(a,b)$	circularly symmetric complex Gaussian RV with a mean and variance of a and b
$\Gamma(.)$	gamma function [40, Eq. (8.310)]
$L_{\ell/2}(.)$	Laguerre polynomial with an order of $\ell/2$ [40, Eq. (8.970.1)]
$\mathrm{erf}(.)$	error function [40, Eq. (8.250.1)]
$\mathrm{erfc}(.)$	complementary error function [40, Eq. (8.250.4)]
${}_1F_1(.,.,.)$	confluent hypergeometric function [40, Eq. (9.210.1)]

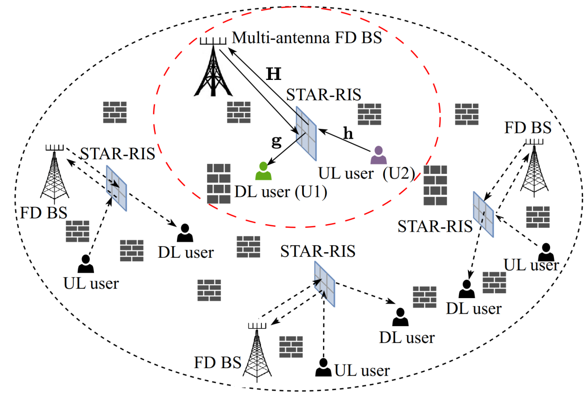

Fig. 1 STAR-RIS assisted terahertz wireless communication network.

II. System Model and Channel Characterization

A. System Model Description

As shown in Fig. 1, we consider a multi-cell THz wireless network and focus on the central cell comprising an FD BS with M transmit and M_r receive antennas, a STAR-RIS with N elements[1], and two single-antenna HD users (U1 and U2). The FD BS simultaneously serves U1 and U2 in the downlink and uplink, respectively. Due to blockage-prone nature of THz systems, we assume that the direct BS-U1/U2 and U1-U2 links are blocked. Moreover, U1 is assumed to be in the reflection space, where it receives the desired signals from the FD BS. Additionally, U2 is assumed to be in the transmission space, where it transmits to the FD BS. Since both users are in the same cell and close to the STAR-RIS, the signals from U2 also reach U1, resulting in non-negligible IUI[2]. The power of signals reflected/transmitted multiple times is ignored due to severe path-loss [13]. Let $\mathbf{H} \in \mathbb{C}^{M\times N}$ given in (1), $\mathbf{h} = (h_1,\dots,h_N) \in \mathbb{C}^{1\times N}$ and $\mathbf{g} = (g_1,\dots,g_N) \in \mathbb{C}^{N\times 1}$ respectively represent the BS-STAR-RIS, U2-STAR-RIS and STAR-RIS-U1 small-scale fading channels, which are assumed to be non-zero mean complex Gaussian RVs as $h_{m,i} \sim \mathcal{CN}(\mu_{h_{m,i}}, \sigma^2_{h_{m,i}})$, $h_i \sim \mathcal{CN}(\mu_{h_i}, \sigma^2_{h_i})$ and $g_i \sim \mathcal{CN}(\mu_{g_i}, \sigma^2_{g_i})$ $\forall i = 1,\dots,N$, $\forall m = 1,\dots,M$ [10], [11], [13].

$$\mathbf{H} = \begin{pmatrix} h_{1,1} & h_{1,2} & \cdots & h_{1,N} \\ h_{2,1} & h_{2,2} & \cdots & h_{2,N} \\ \vdots & \vdots & \ddots & \vdots \\ h_{M,1} & h_{M,2} & \cdots & h_{M,N} \end{pmatrix}. \tag{1}$$

To achieve full-space coverage and serve both users simultaneously, the STAR-RIS is considered under the ES and MS protocols. Therefore, the reflection and transmission coefficient matrices are respectively denoted by $\mathbf{\Theta}^r = \mathrm{diag}\left(\sqrt{\delta_1^r}e^{j\theta_1^r},\dots,\sqrt{\delta_{N_r}^r}e^{j\theta_{N_r}^r}\right)$ and $\mathbf{\Theta}^t = \mathrm{diag}\left(\sqrt{\delta_1^t}e^{j\theta_1^t},\dots,\sqrt{\delta_{N_t}^t}e^{j\theta_{N_t}^t}\right)$, where in the case of ES, $N = N_r = N_t$, and in the case of MS, $N = N_r + N_t$, with N_r and N_t representing the number of elements operating under reflection and transmission modes, respectively. Moreover, $\theta_i^r, \theta_i^t \in [0, 2\pi)$ are the phase shifts, and $\delta_i^r, \delta_i^t \in [0,1]$ are the amplitude coefficients applied by the i-th element. It is to note, θ_i^t and θ_i^r are respectively applied to steer the incident signals towards the BS (in the uplink) and U1 (in the downlink). Furthermore, in the case of MS, the reflecting and transmitting elements can independently configure the phase shifts and amplitude coefficients. However, in the case of ES, based on the boundary conditions, the phase shifts applied by the reflecting and transmitting elements are coupled to each other, such that they should satisfy $|\theta_i^t - \theta_i^r| = \pi/2$ or $3\pi/2$ [35], [36]. Additionally, based on the law of energy conservation, the amplitude coefficients are constrained by $\delta_i^r + \delta_i^t = 1$ [19].

B. Molecular Absorption and Large-scale Path-loss

In the THz band, in addition to large-scale path-loss, atmospheric molecules such as water vapor and oxygen in the propagation medium lead to energy absorption and signal attenuation [11], [12]. Using [13] and [9], the molecular absorption and large-scale path-losses for the desired (reflection) and IUI (transmission) links are respectively expressed as

$$h_r = \sqrt{\frac{G_{\mathrm{BS}}G_r}{64\pi^3}\frac{c}{f d_{\mathrm{BS}} d_r}\exp\left(-\frac{\kappa_\alpha(f)(d_{\mathrm{BS}}+d_r)}{2}\right)}, \tag{2}$$

$$h_t = \sqrt{\frac{G_t G_r}{64\pi^3}\frac{c}{f d_t d_r}\exp\left(-\frac{\kappa_\alpha(f)(d_t+d_r)}{2}\right)}, \tag{3}$$

where G_{BS}, G_r and G_t are respectively the antenna gains of the BS, U1 and U2, f is the carrier frequency, c is the speed of light, and d_{BS}, d_r and d_t are the distances for the BS-STAR-RIS, STAR-RIS-U1 and U2-STAR-RIS links, respectively. Moreover, $\kappa_\alpha(f)$, the absorption coefficient, is obtained from the high resolution transmission (HITRAN) database [9]. In the 0.275-0.4 THz band, it's precisely defined as [12]

$$\kappa_\alpha(f) = \frac{\alpha_1(\rho)}{\alpha_2(\rho) + \left(\frac{f}{100c} - \mathcal{C}_1\right)^2} + \frac{\alpha_3(\rho)}{\alpha_4(\rho) + \left(\frac{f}{100c} - \mathcal{C}_2\right)^2} + \varrho_1 f^3 + \varrho_2 f^2 + \varrho_3 f + \varrho_4, \tag{4}$$

where $\alpha_1(\rho) = 0.2205\rho(0.1303\rho + 0.0294)$, $\alpha_2(\rho) = (0.4093\rho + 0.0925)^2$, $\alpha_3(\rho) = 2.014\rho(0.1702\rho + 0.0303)$,

[1]The Euclidean distance between adjacent elements is considered to be greater than half of the wavelength, which allows us to make the assumption of independent and identically distributed (IID) channels [8], [41].

[2]The effects of ICI signals are negligible due to inter-cell distances, STAR-RIS phase shifts and limiting factors of THz communications [3], [23]–[25], [39]. However, Section III-G demonstrates the applicability of the analytical expressions when accounting for ICI caused by multiple users and BSs.

$\alpha_4(\rho) = (0.537\rho + 0.0956)^2$, $\mathcal{C}_1 = 10.835$ cm^{-1}, $\mathcal{C}_2 = 12.664$ cm^{-1}, $\varrho_1 = 5.54 \times 10^{-37}$ Hz^{-3}, $\varrho_2 = -3.94 \times 10^{-25}$ Hz^{-2}, $\varrho_3 = 9.06 \times 10^{-14}$ Hz^{-1}, $\varrho_4 = -6.36 \times 10^{-3}$, and ρ is the volume mixing ratio of the water vapor which is characterized based on the Buck's equation as [13]

$$\rho = \phi_H \left(\frac{0.06116}{\varrho} + \frac{2.1148}{10^7} \right) \exp\left(\frac{17.502T}{240.97 + T} \right), \quad (5)$$

where ϕ_H, ϱ and T are the relative humidity, the atmospheric pressure and the temperature, respectively.

C. Misalignment Fading Coefficients

In THz communications, the transmit and receive antennas are highly directional which need to be properly aligned. However, in practice, the random buildings sways and environmental factors such as thermal expansions and dynamic wind loads result in beam misalignment or pointing errors at the receiver end [9], [12], [13]. To characterize the misalignment fadings, we assume that all nodes have circular beams [9], [10], [12], [13], where the radius of U1's effective area is denoted by a_r, and the maximum radius of BS's and U2's beams at the distances of d_{BS} and d_t are denoted by $w_{d_{\text{BS}}}$ and w_{d_t}, respectively. Let $h_{p,m}$ and $h_{p,t}$ respectively represent the misalignment fadings affecting the desired and IUI THz signals, where their PDFs are expressed as [12, Eq. (22)]

$$f_{h_{p,m}}(x) = \xi_m A_m^{-\xi_m} x^{\xi_m - 1}, \quad 0 \le x \le A_m, \quad (6)$$

$$f_{h_{p,t}}(x) = \xi_t A_t^{-\xi_t} x^{\xi_t - 1}, \quad 0 \le x \le A_t, \quad (7)$$

with

$$A_m = \left[\text{erf}\left(\sqrt{\frac{\pi}{2}} \frac{a_r}{w_{d_{\text{BS}}}} \right) \right]^2, \quad (8)$$

$$A_t = \left[\text{erf}\left(\sqrt{\frac{\pi}{2}} \frac{a_r}{w_{d_t}} \right) \right]^2, \quad (9)$$

where $\xi_m = \frac{w_m^2}{4\sigma_m^2}$, $\xi_t = \frac{w_t^2}{4\sigma_t^2}$, w_m and w_t are the equivalent beamwidths, σ_m^2 and σ_t^2 are the variances of the pointing errors displacement, and A_m and A_t are the fractions of power collected by U1 under optimal alignment for the desired and IUI links, respectively. Moreover, $w_m^2 = \frac{w_{d_{\text{BS}}}^2 \text{erf}(\chi_m)\sqrt{\pi}}{2\chi_m \exp(-\chi_m^2)}$, $w_t^2 = \frac{w_{d_t}^2 \text{erf}(\chi_t)\sqrt{\pi}}{2\chi_t \exp(-\chi_t^2)}$, $\chi_m = \sqrt{\frac{\pi}{2}} \frac{a_r}{w_{d_{\text{BS}}}}$, and $\chi_t = \sqrt{\frac{\pi}{2}} \frac{a_r}{w_{d_t}}$ [9].

D. Random Foggy Conditions

THz signals are significantly affected by random foggy conditions, and the degree of signal attenuation is determined by fog density, which represents the concentration or amount of atmospheric water droplets and ice crystals within the propagation medium [14]–[16], [18]. Let $h_{f,m}$ and $h_{f,t}$ respectively represent the attenuation due to random fog affecting the desired and IUI signals, which are expressed as [14, Eq. (5)]

$$h_{f,m} = \exp\left(-\frac{\beta\left(d_{\text{BS}} + d_r\right)}{4343} \right). \quad (10)$$

$$h_{f,t} = \exp\left(-\frac{\beta\left(d_t + d_r\right)}{4343} \right). \quad (11)$$

The parameter β represents various levels of random foggy conditions, ranging from light fog and moderate fog to thick fog and the most severe condition, dense fog. The authors in [14] have experimentally shown that β can be modelled by gamma distribution, where its PDF is written as $f_\beta(\beta) = \frac{\beta^{k-1}}{\theta^k \Gamma(k)} e^{-\frac{\beta}{\theta}}$, and the parameters k and θ characterize the fog density. For instance, for light fog $(k, \theta) = (2.32, 13.12)$, for moderate fog $(k, \theta) = (5.49, 12.06)$, for thick fog $(k, \theta) = (6, 23)$, and for dense fog $(k, \theta) = (36.05, 11.91)$ [14], [16].

E. Received Signal and SINR

To study the impacts of IUI and the practical factors of THz, the received signal at the downlink user[3], U1, is expressed as

$$y = \underbrace{\zeta_r \mathbf{g}^H \mathbf{\Theta}^r \mathbf{H} \mathbf{w} x_r}_{\text{Desired signal}} + \underbrace{\zeta_t \mathbf{g}^H \mathbf{\Theta}^t \mathbf{h}\ x_t}_{\text{IUI signal}} + \underbrace{n}_{\text{AWGN}}, \quad (12)$$

where x_r with $\mathbb{E}[|x_r|^2] = P_s$ is the desired data symbol, x_t with $\mathbb{E}[|x_t|^2] = P_t$ is the IUI data symbol, $\mathbf{w}$ is the transmit beamforming vector with $\mathbb{E}\left[||\mathbf{w}||^2\right] = 1$ [42], $n \sim \mathcal{CN}(0, N_0)$ is the additive white Gaussian noise (AWGN), $\zeta_r = h_r h_{p,m} h_{f,m}$ and $\zeta_t = h_t h_{p,t} h_{f,t}$.

In practice, STAR-RISs are equipped with discrete phase shifters, where each element applies quantized phase shift to steer the incident signals towards the desired destinations [36]. Therefore, each phase shift takes a finite number from the set of $\mathcal{S} \triangleq \left\{0, \frac{2\pi}{Q}, \ldots, \frac{2\pi(Q-1)}{Q}\right\}$, where $Q = 2^q$ is the quantization level and q is the number of quantization bits. Although the phases of $h_{m,i}$ and g_i are assumed to be perfectly known at the STAR-RIS, as a result of quantized phase shifts applied by the reflecting elements, an optimal phase shift model is not feasible, and thus the STAR-RIS reflects the desired incident signals with quantization errors. Let $\phi_i^r \triangleq \theta_i^r - \arg(h_{m,i}) - \arg(g_i)$ represent the phase shift quantization errors impacting the desired downlink transmission, which are uniformly distributed in the interval of $[-\pi/Q, \pi/Q]$ [13]. Since for the uplink transmission, the transmitting elements of the STAR-RIS are configured to direct the incident signals of U2 towards the FD BS, the IUI signals randomly arrive at U1, and thus it is assumed that the phase shifts for the IUI signals are random and uniformly distributed in the interval of $[0, 2\pi)$ [13], [43]. Therefore, the instantaneous signal-to-interference-plus-noise ratio (SINR) is expressed as

$$\gamma = \frac{h_r^2 \sum_{m=1}^{M} X_m}{\frac{h_t^2}{\text{SIR}} Y + \frac{1}{\text{SNR}}}, \quad (13)$$

where $\text{SIR} \triangleq \frac{P_s}{P_t}$, $\text{SNR} \triangleq \frac{P_s}{N_0}$, and

$$X_m \triangleq \left| h_{p,m} h_{f,m} \sum_{i=1}^{N} |h_{m,i}|\,|g_i| \sqrt{\delta_i^r} e^{j\phi_i^r} \right|^2. \quad (14)$$

$$Y \triangleq \left| h_{p,t} h_{f,t} \sum_{i=1}^{N} h_i \sqrt{\delta_i^t} e^{j\theta_i^t} g_i \right|^2. \quad (15)$$

[3]In a classical HD downlink system, the received signal is not affected by IUI as U2 does not transmit at the same time as the BS, and the RIS reflection amplitude coefficients are set to unity. Moreover, Section IV compares the performance under both the FD (with ES and MS) and HD scenarios.

III. Performance Analysis

This section characterizes the statistical distributions of X_m and Y, and derives analytical expressions for the ergodic capacity, outage probability, and SER of the downlink user. It also demonstrates the applicability of these expressions to both the uplink scenario and the downlink scenario with ICI caused by multiple users and BSs situated in neighboring cells.

A. Statistical Distributions of X_m and Y

1) Statistical Distribution of X_m: Since X_m given in (14) includes sums and product of a large number of different RVs, deriving its exact PDF is extremely difficult, if not impossible. Nonetheless, by exploiting the orthogonality of Laguerre polynomials on the positive real axis, several studies have shown that the distribution of a positive RV, whose PDF has a single maximum with fast-decaying tails, can be approximated by the Laguerre polynomial expansion, which is a moment-matching approximation method (e.g. [6], [37], [44]–[47]). Therefore, to approximate the PDF of X_m, let $X_m \triangleq h_{p,m}^2 h_{f,m}^2 \lambda_m$, where $\lambda_m \triangleq \lambda_R^2 + \lambda_I^2$ with $\lambda_R \triangleq \sum_{i=1}^{N} |h_{m,i}| |g_i| \sqrt{\delta_i^r} \cos\phi_i^r$ and $\lambda_I \triangleq \sum_{i=1}^{N} |h_{m,i}| |g_i| \sqrt{\delta_i^r} \sin\phi_i^r$. Since $h_{p,m}$, $h_{f,m}$, and λ_m are positive RVs, it follows that X_m is also a positive RV. Thus, the PDF of X_m can be approximated using the first branch of the Laguerre expansion as [47, Eq. (2.76)]

$$f_{X_m}(X_m) \approx \frac{X_m^{\xi_x} \, e^{-\frac{X_m}{\eta_x}}}{\eta_x^{\xi_x+1} \Gamma(\xi_x+1)}, \tag{16}$$

where $\xi_x = \mu_x^2/\sigma_x^2 - 1$, $\eta_x = \sigma_x^2/\mu_x$ [47, Eq. (2.74)], and μ_x and σ_x^2 are the mean and variance of X_m, respectively.

In addition, since $h_{p,m}^2$, $h_{f,m}^2$ and λ_m are independent RVs, the mean and variance of X_m are respectively written as

$$\mu_x = \mathbb{E}\left[h_{p,m}^2\right] \mathbb{E}\left[h_{f,m}^2\right] \mathbb{E}\left[\lambda_m\right], \tag{17}$$

$$\sigma_x^2 = \mathbb{E}\left[h_{p,m}^4\right] \mathbb{E}\left[h_{f,m}^4\right] \left(\mathbb{V}\left[\lambda_m\right] + \mathbb{E}^2\left[\lambda_m\right]\right) - \mu_x^2, \tag{18}$$

where the corresponding mean, moments and variance terms required for (17) and (18) are provided in Appendix A. ■

2) Statistical Distribution of Y: Similar to X_m, deriving the exact PDF of Y is also extremely difficult. Let $Y \triangleq h_{p,t}^2 h_{f,t}^2 |\lambda|^2$ with $\lambda \triangleq \sum_{i=1}^{N} h_i \sqrt{\delta_i^t} e^{j\theta_i^t} g_i$, which is a positive RV. Therefore, its PDF can also be approximated by the expansion of Laguerre polynomials as [47, Eq. (2.76)]

$$f_Y(Y) \approx \frac{Y^{\xi_y} \, e^{-\frac{Y}{\eta_y}}}{\eta_y^{\xi_y+1} \Gamma(\xi_y+1)}, \tag{19}$$

where $\xi_y = \mu_y^2/\sigma_y^2 - 1$, $\eta_y = \sigma_y^2/\mu_y$, and μ_y and σ_y^2 are the mean and variance of Y written as

$$\mu_y = \mathbb{E}\left[h_{p,t}^2\right] \mathbb{E}\left[h_{f,t}^2\right] \mathbb{E}\left[|\lambda|^2\right], \tag{20}$$

$$\sigma_y^2 = \mathbb{E}\left[h_{p,t}^4\right] \mathbb{E}\left[h_{f,t}^4\right] \left(\mathbb{V}\left[|\lambda|^2\right] + \mathbb{E}^2\left[|\lambda|^2\right]\right) - \mu_y^2, \tag{21}$$

where the corresponding mean, moments and variance terms required for (20) and (21) are provided in Appendix B. ■

In order to validate the accuracy of the approximated PDFs given in (16) and (19), we compare them with their exact PDFs through numerical and computer simulation results. The results are obtained for $d_{\text{BS}} = 15$ m, $d_t = d_r = 10$ m, $\delta^t = \delta^r = 0.5$, $Q = 2$, $\mu_{h_m} = \mu_h = \mu_g = 1$, $\sigma_{h_m}^2 = \sigma_h^2 = \sigma_g^2 = 1$, $k = 6$, $\theta = 23$, $N = \{10, 20, 30, 50, 100\}$, $\sigma_m = \sigma_t = 0.01$ m, and the normalized beamwidths of $w_{d_{\text{BS}}}/a_r = w_{d_t}/a_r = 6$. Fig. 2 illustrates a comparison between the approximated and exact PDFs of X_m for different numbers of STAR-RIS elements. In particular, Fig. 2 (a), Fig. 2 (b), and Fig. 2 (c) present the comparisons for $N = \{10, 20\}$, $N = \{30, 50\}$, and $N = 100$, respectively. Moreover, Fig. 3 provides a comparison between the approximated and exact PDFs of Y for various numbers of STAR-RIS elements. Specifically, Fig. 3 (a), Fig. 3 (b), Fig. 3 (c), and Fig. 3 (d) present the comparisons for $N = 10$, $N = 30$, $N = 50$, and $N = 100$, respectively.

As shown in the figures, for different numbers of STAR-RIS elements, the PDFs of the positive RVs, X_m and Y, exhibit a single maximum and fast-decaying tails. This observation confirms that they can be approximated by the Laguerre expansion [6], [37], [44]–[47]. It is also shown that for a small number of STAR-RIS elements, i.e. $N = 10$, the approximated PDFs are less accurate, but they can still be utilized. In contrast, for a moderate number of STAR-RIS elements, i.e. $N = 30$, the approximations exhibit great agreement with the exact simulated PDFs, where the accuracy is significantly improved by increasing the number of elements to $N = 50$ and $N = 100$. Therefore, it confirms that the PDFs provided in (16) and (19), converge effectively when the number of STAR-RIS elements equals or exceeds 30 ($N \geq 30$). This highlights the accuracy and appropriateness of the Laguerre expansion as an effective approximation for practical STAR-RISs that are equipped with a large number of elements.

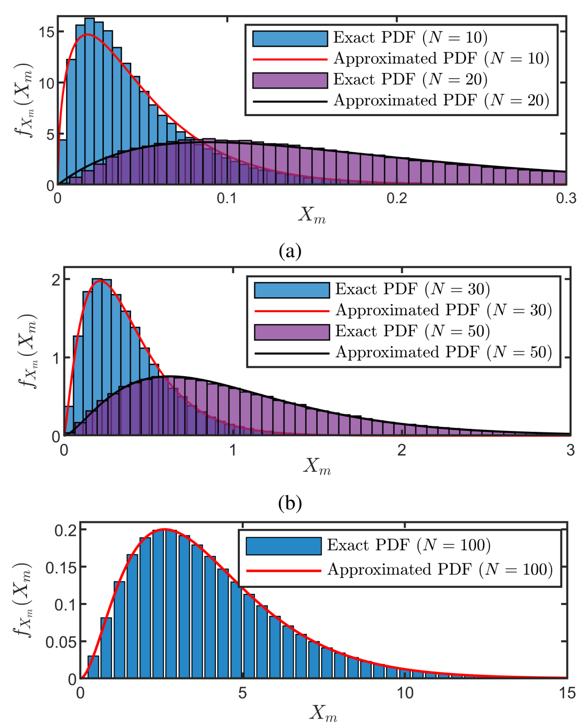

(a)

(b)

(c)

Fig. 2 Comparison of exact and approximated PDFs of X_m. (a) $N = \{10, 20\}$ (b) $N = \{30, 50\}$ (c) $N = 100$.

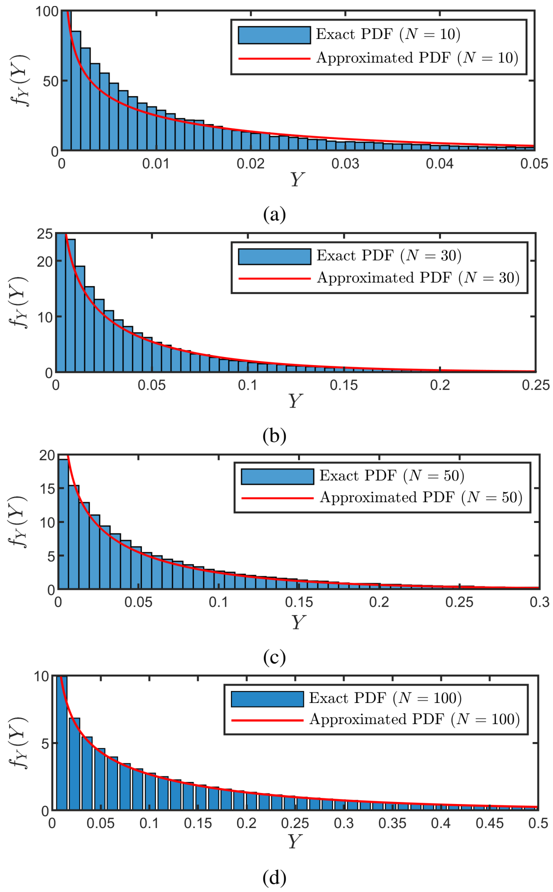

Fig. 3 Comparison of exact and approximated PDFs of Y. (a) $N = 10$ (b) $N = 30$ (c) $N = 50$ (d) $N = 100$.

B. Ergodic Capacity

In order to evaluate the capacity performance, the following lemma is presented.

Lemma 1. Using the SINR given in (13), the ergodic capacity, $C = \mathbb{E}\left[\log_2\left(1+\gamma\right)\right]$, is obtained as

$$C = \frac{1}{\ln 2}\int_0^{\infty}\frac{\left[1-\frac{1}{\left(1+sh_r^2\eta_x\right)^{M(\xi_x+1)}}\right]}{s\left(1+\frac{sh_t^2\eta_y}{\mathrm{SIR}}\right)^{\xi_y+1}}e^{-\frac{s}{\mathrm{SNR}}}\,\mathrm{d}s. \quad (22)$$

It is to note, (22) is efficiently evaluated via numerical integration. Alternatively, a closed-form expression for (22) in terms of the sample points and weights factors of the Laguerre orthogonal polynomial is expressed as [48, Eq. (25.4.45)]

$$C = \frac{1}{\ln 2}\sum_{\ell=1}^{L}\frac{\Omega_\ell\left[1-\frac{1}{\left(1+\mathcal{G}_\ell h_r^2\eta_x\mathrm{SNR}\right)^{M(\xi_x+1)}}\right]}{\mathcal{G}_\ell\left(1+\frac{\mathcal{G}_\ell h_t^2\eta_y\mathrm{SNR}}{\mathrm{SIR}}\right)^{\xi_y+1}}+R_L, \quad (23)$$

where $\mathcal{G}_\ell$ and Ω_ℓ are respectively the sample points and the weights factors tabulated in [48, TABLE (25.9)], $R_L = \frac{(L!)^2}{(2L)!}f^{(2L)}\left(t\right)$ is a remainder, and $f^{(2L)}\left(t\right)$ is the $2L$-th derivative of $f\left(t\right) = \left[1-\frac{1}{\left(1+t\ h_r^2\eta_x\mathrm{SNR}\right)^{M(\xi_x+1)}}\right]t^{-1}\left(1+\frac{th_t^2\eta_y\mathrm{SNR}}{\mathrm{SIR}}\right)^{-\xi_y-1}$.

It can be written that $\lim\limits_{L\to\infty}R_L = \lim\limits_{L\to\infty}\frac{(L!)^2}{(2L)!}f^{(2L)}\left(t\right)\approx 0$. This is because as we increase L, both the term $\frac{(L!)^2}{(2L)!}$ and the higher-order derivative, $f^{(2L)}\left(t\right)$, decrease significantly, causing the remainder to become negligible.

Proof: By exploiting [49, Eq. (4)] and (13), the ergodic capacity is written as

$$\begin{aligned}C &= \mathbb{E}\left[\log_2\left(1+\frac{h_r^2\sum_{m=1}^{M}X_m}{\frac{h_t^2}{\mathrm{SIR}}Y+\frac{1}{\mathrm{SNR}}}\right)\right]\\ &= \frac{1}{\ln 2}\mathbb{E}\left[\int_0^{\infty}\frac{1}{z}\left(1-e^{-z\frac{h_r^2\sum_{m=1}^{M}X_m}{\frac{h_t^2}{\mathrm{SIR}}Y+\frac{1}{\mathrm{SNR}}}}\right)e^{-z}\mathrm{d}z\right]. \quad (24)\end{aligned}$$

Let $z \triangleq s\left(\frac{h_t^2}{\mathrm{SIR}}Y+\frac{1}{\mathrm{SNR}}\right)$, and thus (24) is rewritten as

$$C = \frac{1}{\ln 2}\mathbb{E}\left[\int_0^{\infty}\frac{e^{-\frac{s}{\mathrm{SNR}}}}{s}\left(1-e^{-sh_r^2\sum_{m=1}^{M}X_m}\right)e^{-s\frac{h_t^2Y}{\mathrm{SIR}}}\mathrm{d}s\right]. \quad (25)$$

By virtue of Fubini's and Tonelli's theorems, it is possible to exchange the integral and expectation in (25), as the integrand is positive and exists for all $s > 0$ [49], [50]. Moreover, by virtue of [13], [38, Appendix A], [43] and [51, Appendix B], for a sufficiently large number of STAR-RIS elements, X_m and Y are assumed to be independent RVs. As a result, (25) can be equivalently written as

$$C = \frac{1}{\ln 2}\int_0^{\infty}\frac{e^{-\frac{s}{\mathrm{SNR}}}}{s}\left[1-\mathcal{M}_X(-s)\right]\mathcal{M}_Y(-s)\mathrm{d}s, \quad (26)$$

where $\mathcal{M}_X(-s)$ is the MGF of $X \triangleq h_r^2\sum_{m=1}^{M}X_m$, and $\mathcal{M}_Y(-s)$ is the MGF of Y.

Since X_m and Y are approximated by the Laguerre expansion, using [44, Eq. (13)], the MGFs of X and Y are respectively written as

$$\mathcal{M}_X(-s) = \mathbb{E}\left[e^{-sh_r^2\sum_{m=1}^{M}X_m}\right] = \left(1+sh_r^2\eta_x\right)^{-M(\xi_x+1)}. \quad (27)$$

$$\mathcal{M}_Y(-s) = \mathbb{E}\left[e^{\frac{-sh_t^2Y}{\mathrm{SIR}}}\right] = \left(1+\frac{sh_t^2\eta_y}{\mathrm{SIR}}\right)^{-\xi_y-1}. \quad (28)$$

Finally, by substituting the MGF expressions, (27) and (28), into (26), the expression given in (22) is obtained. ■

C. Outage Probability

The following lemma is provided which facilitates an accurate evaluation of the outage probability.

Lemma 2. Let γ_{th} represent the SINR threshold, and thus the outage probability, $P_o = \mathrm{P_r}\left(\gamma \leq \gamma_{th}\right)$, is obtained as

$$P_o = \frac{2}{\pi}\int_0^{\infty}\frac{\mathrm{Re}\left\{\Phi_X\left(\omega\right)\right\}\mathrm{Im}\left\{\Phi_Y\left(\omega\right)\right\}}{\omega}\mathrm{d}\omega, \quad (29)$$

where $\Phi_Y\left(\omega\right) = e^{j\frac{\omega\gamma_{th}}{\mathrm{SNR}}}\left(1-j\frac{\omega\gamma_{th}h_t^2\eta_y}{\mathrm{SIR}}\right)^{-\xi_y-1}$ and $\mathrm{Re}\left\{\Phi_X\left(\omega\right)\right\}$ is given in (33).

The integral of (29) is easily evaluated by numerical integration, which is much faster than Monte-Carlo simulations. Alternatively, for a more efficient numerical integration, by interchange of $\omega = \tan\alpha$ in (29), it is equivalently written as

$$P_o = \frac{4}{\pi}\int_0^{\frac{\pi}{2}}\frac{\mathrm{Re}\left\{\Phi_X\left(\tan\alpha\right)\right\}\mathrm{Im}\left\{\Phi_Y\left(\tan\alpha\right)\right\}}{\sin 2\alpha}\mathrm{d}\alpha. \quad (30)$$

Proof: Since the SINR given in (13) is the ratio of positive RVs, we first need to derive the conditional outage probability. In addition, according to [52, Eq. (5)], using the Gil-Pelaez's inversion formula for non-negative RVs, the probability of a positive RV, $x > 0$, can be computed as $\mathrm{P_r}(x \leq a) = \frac{2}{\pi}\int_0^\infty \frac{\mathrm{Re}\{\Phi_x(\omega)\}}{\omega}\sin(\omega a)\mathrm{d}\omega$. Therefore, the outage probability conditioned on Y is expressed as

$$\begin{aligned} P_{o|Y} &= \mathrm{P_r}\left(\frac{h_r^2\sum_{m=1}^{M}X_m}{\frac{h_t^2}{\mathrm{SIR}}Y+\frac{1}{\mathrm{SNR}}} \leq \gamma_{th}|Y\right) \\ &= \mathrm{P_r}\left(h_r^2\sum_{m=1}^{M}X_m \leq \gamma_{th}\left(\frac{h_t^2}{\mathrm{SIR}}Y+\frac{1}{\mathrm{SNR}}\right)\Big|Y\right) \\ &= \frac{2}{\pi}\int_0^\infty \frac{\mathrm{Re}\{\Phi_X(\omega)\}\sin\left[\omega\gamma_{th}\left(\frac{h_t^2}{\mathrm{SIR}}Y+\frac{1}{\mathrm{SNR}}\right)\right]}{\omega}\mathrm{d}\omega, \end{aligned} \tag{31}$$

where $\mathrm{Re}\{\Phi_X(\omega)\} = \mathrm{Re}\left\{\mathbb{E}\left[e^{j\omega h_r^2\sum_{m=1}^{M}X_m}\right]\right\}$ represents the real part of the CHF of $X \triangleq h_r^2\sum_{m=1}^{M}X_m$.

From (27), the MGF of X is written as $\mathcal{M}_X(-s) = \left(1+sh_r^2\eta_x\right)^{-M(\xi_x+1)}$, and thus by applying the inverse Laplace transform [48, Eq. (29.3.11)], its PDF is obtained as

$$f_X(X) = \frac{X^{M(\xi_x+1)-1}e^{-\frac{X}{h_r^2\eta_x}}}{\Gamma\left(M\left(\xi_x+1\right)\right)\left(h_r^2\eta_x\right)^{M(\xi_x+1)}}. \tag{32}$$

By applying [40, Eq. (3.944.6)], $\mathrm{Re}\{\Phi_X(\omega)\}$ is derived as

$$\begin{aligned} \mathrm{Re}\{\Phi_X(\omega)\} &= \int_0^\infty \cos(\omega X)f_X(X)\mathrm{d}X \\ &= \frac{\int_0^\infty \cos(\omega X)X^{M(\xi_x+1)-1}e^{-\frac{X}{h_r^2\eta_x}}\mathrm{d}X}{\Gamma\left(M\left(\xi_x+1\right)\right)\left(h_r^2\eta_x\right)^{M(\xi_x+1)}} \\ &= \frac{\cos\left(M\left(\xi_x+1\right)\arctan\left(\omega h_r^2\eta_x\right)\right)}{\left(1+\omega^2h_r^4\eta_x^2\right)^{\frac{M(\xi_x+1)}{2}}}. \end{aligned} \tag{33}$$

In order to derive the unconditional outage probability, we need to take the expectation of (31) with respect to Y. Moreover, the integrand of (31) for $\omega > 0$ exists and is positive, and thus based on the Fubini's and Tonelli's theorems, the expectation and integral are interchangeable [50]. As a result, the unconditional outage probability is expressed as

$$P_o = \frac{2}{\pi}\int_0^\infty \frac{\mathrm{Re}\{\Phi_X(\omega)\}}{\omega}\mathbb{E}\left[\sin\left(\frac{\omega\gamma_{th}h_t^2Y}{\mathrm{SIR}}+\frac{\omega\gamma_{th}}{\mathrm{SNR}}\right)\right]\mathrm{d}\omega, \tag{34}$$

where $\mathrm{Im}\{\Phi_Y(\omega)\} = \mathbb{E}\left[\sin\left(\frac{\omega\gamma_{th}h_t^2Y}{\mathrm{SIR}}+\frac{\omega\gamma_{th}}{\mathrm{SNR}}\right)\right]$ is the imaginary part of the CHF of Y, and similar to $\mathcal{M}_Y(-s)$ given in (28), we can write that $\Phi_Y(\omega) = e^{j\frac{\omega\gamma_{th}}{\mathrm{SNR}}}\left(1-j\frac{\omega\gamma_{th}h_t^2\eta_y}{\mathrm{SIR}}\right)^{-\xi_y-1}$, and thus the outage probability expression given in (29) is obtained. ∎

D. Symbol Error Rate (SER)

By exploiting [42, Eq. (22)] and (13), the average SER for different coherent modulation schemes can be expressed as

$$P_e \approx a\mathbb{E}\left[\mathrm{erfc}\left(\sqrt{\frac{bh_r^2\sum_{m=1}^{M}X_m}{\frac{h_t^2}{\mathrm{SIR}}Y+\frac{1}{\mathrm{SNR}}}}\right)\right], \tag{35}$$

where a and b are modulation related constants. For instance, for binary phase shift keying (BPSK) $a = b = 1$, for quadrature phase shift keying (QPSK) $a = 2$ and $b = 1$, for $\mathcal{M}$-ary phase shift keying (MPSK) $a = 2$ and $b = \sin^2(\pi/\mathcal{M})$, for $\mathcal{M}$-ary pulse amplitude modulation (MPAM) $a = 2 - 2/\mathcal{M}$ and $b = 3/(\mathcal{M}^2 - 1)$, and for square $\mathcal{M}$-ary quadrature amplitude modulation (MQAM) $a = 4\left(1-1/\sqrt{\mathcal{M}}\right)$ and $b = 3/\left(2\mathcal{M}-2\right)$ [53, TABLE 6.1].

Lemma 3. The average SER of the system given in (35) is accurately evaluated as

$$P_e = 2a\int_0^\infty \frac{1-e^{\frac{-\omega^2}{4\mathrm{SNR}}}\left(1+\frac{\omega^2h_t^2\eta_y}{4\mathrm{SIR}}\right)^{-\xi_y-1}}{\pi\omega}\mathrm{Im}\{\Phi_\varphi(\omega)\}\mathrm{d}\omega, \tag{36}$$

with

$$\mathrm{Im}\{\Phi_\varphi(\omega)\} = \frac{2\omega\sqrt{\mathcal{K}_1}\Gamma\left(\mathcal{K}_2\right)\ {}_1F_1\left(\mathcal{K}_2,\frac{3}{2};-\omega^2\mathcal{K}_1\right)}{\Gamma\left(\mathcal{K}_2-\frac{1}{2}\right)}, \tag{37}$$

where $\mathcal{K}_1 = \frac{bh_r^2\eta_x}{4}$ and $\mathcal{K}_2 = M\left(\xi_x+1\right)+1/2$.

The integral of (36) is easily assessed through numerical integration. Furthermore, by interchange of $\omega = \tan\alpha$ in (36), and after some algebraic manipulations, a more suitable expression for numerical integration is obtained as

$$P_e = \int_0^{\frac{\pi}{2}} \frac{4a\,\mathrm{Im}\{\Phi_\varphi(\tan\alpha)\}\left[1-\frac{e^{-\frac{\tan^2\alpha}{4\mathrm{SNR}}}}{(1+\mathcal{K}(\alpha))^{\xi_y+1}}\right]}{\pi\sin 2\alpha}\mathrm{d}\alpha, \tag{38}$$

where $\mathcal{K}(\alpha) = \frac{\tan^2\alpha h_t^2\eta_y}{4\mathrm{SIR}}$.

Proof: Based on the convolution theorem for the Fourier sine transform, the average of an absolutely integrable function, $g(x)$, with a PDF of $f_x(x)$ can be obtained by $\mathbb{E}\left[g(x)\right] = \frac{2}{\pi}\int_0^\infty G_s(\omega)\,\mathrm{Im}\{\Phi_x(\omega)\}\mathrm{d}\omega$, where $G_s(w) = \int_0^\infty \sin(\omega x)g(x)\mathrm{d}x$ is the Fourier sine transform of $g(x)$ and $\Phi_x(\omega)$ is the CHF of x [54]. Therefore, let $\varphi \triangleq \sqrt{bh_r^2\sum_{m=1}^{M}X_m}$ and $\vartheta \triangleq \sqrt{\frac{h_t^2}{\mathrm{SIR}}Y+\frac{1}{\mathrm{SNR}}}$, the SER conditioned on ϑ is written as

$$\begin{aligned} P_{e|\vartheta} &= a\mathbb{E}\left[\mathrm{erfc}\left(\frac{\varphi}{\vartheta}\Big|\vartheta\right)\right] \\ &= \frac{2a}{\pi}\int_0^\infty \underbrace{\left[\int_0^\infty \sin(\omega\varphi)\mathrm{erfc}\left(\frac{\varphi}{\vartheta}\right)\mathrm{d}\varphi\right]}_{G_s(\omega)}\mathrm{Im}\{\Phi_\varphi(\omega)\}\mathrm{d}\omega \\ &= \frac{2a}{\pi}\int_0^\infty \frac{1-e^{-\frac{\omega^2\vartheta^2}{4}}}{\omega}\mathrm{Im}\{\Phi_\varphi(\omega)\}\mathrm{d}\omega, \end{aligned} \tag{39}$$

where the integral of $G_s(\omega)$ is evaluated by [55, Eq. (4.5.5)].

By substituting $\vartheta \triangleq \sqrt{\frac{h_t^2}{\mathrm{SIR}}Y+\frac{1}{\mathrm{SNR}}}$ into (39), and then taking the expectation of (39) with respect to Y, the unconditional SER is written as

$$P_e = \frac{2a}{\pi}\int_0^\infty \frac{1-e^{\frac{-\omega^2}{4\mathrm{SNR}}}\mathbb{E}\left[e^{\frac{-\omega^2h_t^2Y}{4\mathrm{SIR}}}\right]}{\omega}\mathrm{Im}\{\Phi_\varphi(\omega)\}\mathrm{d}\omega, \tag{40}$$

where $\mathbb{E}\left[e^{\frac{-\omega^2h_t^2Y}{4\mathrm{SIR}}}\right] = \mathcal{M}_Y\left(\frac{-\omega^2h_t^2}{4\mathrm{SIR}}\right) = \left(1+\frac{\omega^2h_t^2\eta_y}{4\mathrm{SIR}}\right)^{-\xi_y-1}$.

On the other hand, since $\varphi = \sqrt{bh_r^2 \sum_{m=1}^{M} X_m} = \sqrt{bX}$, where the PDF of X is given in (32). As a result, the PDF of φ is obtained through $f_\varphi(\varphi) = \frac{2\varphi}{b} f_X(\frac{\varphi^2}{b})$ as

$$f_\varphi\left(\varphi\right) = \frac{2\varphi^{2M(\xi_x+1)-1} e^{-\frac{\varphi^2}{bh_r^2\eta_x}}}{\Gamma\left(M(\xi_x+1)\right)\left(bh_r^2\eta_x\right)^{M(\xi_x+1)}}. \tag{41}$$

Therefore, using (41), $\mathrm{Im}\left\{\Phi_\varphi(\omega)\right\}$ is derived as

$$\begin{aligned}\mathrm{Im}\left\{\Phi_\varphi(\omega)\right\} &= \int_0^\infty \sin\left(\omega\varphi\right) f_\varphi\left(\varphi\right) \mathrm{d}\varphi \\ &= \frac{2\int_0^\infty \sin\left(\omega\varphi\right)\varphi^{2M(\xi_x+1)-1} e^{-\frac{\varphi^2}{bh_r^2\eta_x}} \mathrm{d}\varphi}{\Gamma\left(M(\xi_x+1)\right)\left(bh_r^2\eta_x\right)^{M(\xi_x+1)}}.\end{aligned} \tag{42}$$

By applying [40, Eq. (3.952.7)] and [40, Eq. (9.212.1)], the integral of (42) is evaluated, which yields (37). Finally, by substituting the corresponding MGF and CHF expressions into (40), the SER expression given in (36) is obtained. ■

E. System Performance in the High-SNR Regime

In order to gain further insights into the system performance, we analyze the performance metrics and SINR behaviour in the high-SNR regime. Therefore, for $\mathrm{SNR} \to \infty$, the SINR expression given in (13) takes the following form.

$$\begin{aligned}\gamma^\infty &= \lim_{\mathrm{SNR}\to\infty} \frac{h_r^2 \sum_{m=1}^{M} X_m}{\frac{h_t^2}{\mathrm{SIR}} Y + \frac{1}{\mathrm{SNR}}} \\ &= \frac{h_r^2 \sum_{m=1}^{M} X_m}{\frac{h_t^2}{\mathrm{SIR}} Y}.\end{aligned} \tag{43}$$

By exploiting (43) and following the same steps as used in Lemma 1, Lemma 2, and Lemma 3, we obtain the ergodic capacity, outage probability, and SER in the high-SNR regime, given as (44), (45), and (46), respectively.

$$C^\infty = \frac{1}{\ln 2}\int_0^\infty \frac{\left[1 - \frac{1}{\left(1+sh_r^2\eta_x\right)^{M(\xi_x+1)}}\right]}{s\left(1+\frac{sh_t^2\eta_y}{\mathrm{SIR}}\right)^{\xi_y+1}} \mathrm{d}s. \tag{44}$$

$$P_o^\infty = \int_0^{\frac{\pi}{2}} \frac{4\,\mathrm{Re}\left\{\Phi_X\left(\tan\alpha\right)\right\}\mathrm{Im}\left\{\frac{1}{\left(1-j\mathcal{I}(\alpha)\right)^{\xi_y+1}}\right\}}{\pi\sin 2\alpha} \mathrm{d}\alpha, \tag{45}$$

where $\mathrm{Re}\left\{\Phi_X\left(\tan\alpha\right)\right\}$ is given in (33), and $\mathcal{I}(\alpha) = \frac{\gamma_{th} h_t^2 \eta_y \tan\alpha}{\mathrm{SIR}}$.

$$P_e^\infty = \int_0^{\frac{\pi}{2}} \frac{4a\,\mathrm{Im}\left\{\Phi_\varphi(\tan\alpha)\right\}\left[1 - \frac{1}{\left(1+\mathcal{K}(\alpha)\right)^{\xi_y+1}}\right]}{\pi\sin 2\alpha} \mathrm{d}\alpha, \tag{46}$$

where $\mathrm{Im}\left\{\Phi_\varphi(\omega)\right\}$ is given in (37), and $\mathcal{K}(\alpha) = \frac{\tan^2\alpha h_t^2\eta_y}{4\mathrm{SIR}}$.

Remark 1. *From (43), (44), (45) and (46), it is evident that the asymptotic SINR and performance metrics are independent of SNR. This independence indicates that due to IUI, the system performance in the high-SNR regime reaches a limit, which cannot be improved by increasing the SNR. However, it can be scaled by other factors, such as the number of antennas and STAR-RIS elements, and the STAR-RIS amplitude coefficients.*

F. Uplink Transmission Scenario

We assume that the FD BS is equipped with M_r receive antennas, and employs the maximum ratio combining technique. In the uplink scenario, U2 transmits signals to the FD BS by utilizing the transmitting elements of the STAR-RIS. The FD BS also receives SI signals caused by its transmit antennas. Without loss of generality, it is assumed that the FD BS applies SIC to either completely eliminate or significantly mitigate the SI signals [5], [7], [22], [26]. In the later case, the effect of imperfect SIC is commonly modeled as a zero-mean complex Gaussian RV, that acts as an additive noise power [5], [7], [22], [26]. Therefore, let $\mathcal{R}_{\mathrm{SI}} \sim \mathcal{CN}(0, \sigma_s^2)$ represent the residual SI arising due to imperfect SIC, where $\sigma_s^2 = vP_s$ is the residual SI power, P_s is the power of the FD BS, and $v > 0$ is a parameter that characterizes the severity of the residual SI [5], [7]. As a result, the received signal after the SIC process at the FD BS is expressed as

$$y = \hat{\zeta}_t \mathbf{w}_r^H \mathbf{H}\mathbf{\Theta}^t \mathbf{h}\; x_t + \mathcal{R}_{\mathrm{SI}} + \mathbf{n}, \tag{47}$$

where $\hat{\zeta}_t = \hat{h}_t \hat{h}_{p,m} \hat{h}_{f,m}$, $\mathbf{n} \in \mathbb{C}^{M_r \times 1}$ is the AWGN with mean zero and variance N_0, and $\mathbf{w}_r \in \mathbb{C}^{M_r\times 1}$ is the receiving combining vector with $\mathbb{E}\left[||\mathbf{w}_r||^2\right] = 1$. Moreover, $\hat{h}_t$, $\hat{h}_{p,m}$, and $\hat{h}_{f,m}$ represent the the path-loss with molecular absorption, the beam misalignment, and the random fog, which can be expressed similar to (3), (6), and (10), respectively.

When the STAR-RIS is enabled with the ES protocol, the phase shifts applied for the downlink and uplink are coupled to each other, such that they should satisfy $|\theta_i^t - \theta_i^r| \in \{\pi/2, 3\pi/2\}$ [35], [36]. Moreover, the authors in [36] have shown that when considering optimal phase shifts for the reflecting elements, due to the coupled phase shifts, the incident signals are transmitted with errors—referred to as selection errors[4]—that exhibit one-bit phase errors with uniform distribution, i.e., $\theta_i^{\mathrm{sel}} \sim U\left(-\pi/2, \pi/2\right)$ [36]. Since we consider a practical STAR-RIS with discrete phase shifters, similar to the downlink scenario discussed in Section II-E, the uplink transmission is also impacted by phase shift quantization errors, i.e. $\phi_i^t \triangleq \theta_i^t - \arg(h_{m,i}) - \arg(h_i)$, which are uniformly distributed in the interval of $[-\pi/Q, \pi/Q]$ [13]. Therefore, the combined phase errors are written as $\Psi_i^t = \phi_i^t + \theta_i^{\mathrm{sel}}$. As a result, by exploiting the received signal given in (47), the instantaneous received SNR at the FD BS is expressed as

$$\gamma = \frac{P_t \hat{h}_t^2 \sum_{m=1}^{M_r} X_m}{\sigma_s^2 + N_0}, \tag{48}$$

where $X_m \triangleq \left|\hat{h}_{p,m}\hat{h}_{f,m}\sum_{i=1}^{N}|h_{m,i}|\,|h_i|\sqrt{\delta_i^t} e^{j\Psi_i^t}\right|^2$.

By comparing (13) and (48), it is obvious that in the uplink scenario, the RV Y does not exist (i.e. $Y = 0$). Therefore, by setting $\mathrm{SNR} \triangleq \frac{P_t}{\sigma_s^2+N_0}$, and the MGF and CHF terms as $\mathcal{M}_Y(-s) = \mathbb{E}[e^{-sY}] = 1$ and $\Phi_Y(\omega) = \mathbb{E}[e^{j\omega Y}] = 1$ in Lemma 1, Lemma 2, and Lemma 3, the ergodic capacity, outage probability, and SER of the FD BS are readily obtained. Moreover, by considering the combined

[4] In the MS protocol, since one group of STAR-RIS elements only reflects and the other only transmits, the phase shifts for the downlink and uplink can be independently configured, and thus the selection errors do not exist.

phase errors due to quantization and selection errors, the mean and variance given in (53) and (54) are applicable, but with $\mathcal{F}1 = \mathbb{E}\left[\cos \Psi_i^t\right] = \mathbb{E}\left[\cos \phi_i^t \cos \theta_i^{\text{sel}}\right] - \mathbb{E}\left[\sin \phi_i^t \sin \theta_i^{\text{sel}}\right] = \frac{2Q}{\pi^2} \sin\left(\frac{\pi}{Q}\right)$ and $\mathcal{F}2 = \mathbb{E}\left[\cos 2\Psi_i^t\right] = \mathbb{E}\left[\cos 2\phi_i^t \cos 2\theta_i^{\text{sel}}\right] - \mathbb{E}\left[\sin 2\phi_i^t \sin 2\theta_i^{\text{sel}}\right] = \frac{\sin(2\pi/Q)}{2\pi/Q} \frac{\sin(\pi)}{\pi} = 0$, which are obtained by exploiting [13] and [42].

G. Downlink Transmission with Inter-cell Interference

As shown in Fig. 1, we consider the downlink transmission in the presence of IUI caused by U2 and ICI caused by multiple users and BSs located in neighboring cells. It is assumed that the reflecting and transmitting elements of the STAR-RIS randomly reflect and transmit the signals of L_r and L_t ICI interferers, respectively. It is also assumed that each interfering user/BS located in the vicinity of the reflection space is equipped with K_1 transmit antennas, and similarly, each interfering user/BS located in the vicinity of the transmission space is equipped with K_2 transmit antennas. Moreover, let $\mathbf{H}_l \in \mathbb{C}^{K_1 \times N}$ $\forall l = 1, \ldots, L_r$ represent the fading channels between the STAR-RIS and interfering users/BSs located in the vicinity of the reflection space, and $\mathbf{H}_{\hat{\ell}} \in \mathbb{C}^{K_2 \times N}$ $\forall \ell = 1, \ldots, L_t$ represent the fading channels between the STAR-RIS and interfering users/BSs located in the vicinity of the transmission space. Therefore, the combined received signal at U1 is expressed as

$$y = \underbrace{\zeta_r \mathbf{g}^H \mathbf{\Theta}^r \mathbf{H} \mathbf{w} x_r}_{\text{Desired signal}} + \underbrace{\zeta_t \mathbf{g}^H \mathbf{\Theta}^t \mathbf{h}\ x_t}_{\text{IUI signal}} + \underbrace{\sum_{l=1}^{L_r} \zeta_l \mathbf{g}^H \mathbf{\Theta}^r \mathbf{H}_l \mathbf{w}_l x_l}_{\text{ICI reflected by STAR-RIS}}$$
$$+ \underbrace{\sum_{\hat{\ell}=1}^{L_t} \zeta_{\hat{\ell}} \mathbf{g}^H \mathbf{\Theta}^t \mathbf{H}_{\hat{\ell}} \mathbf{w}_{\hat{\ell}} x_{\hat{\ell}}}_{\text{ICI transmitted by STAR-RIS}} + \underbrace{n}_{\text{AWGN}}, \tag{49}$$

where $\zeta_l = h_{r,l} h_{p,n,l} h_{f,n,l}$, $\zeta_{\hat{\ell}} = h_{t,\hat{\ell}} h_{p,\tau,\hat{\ell}} h_{f,\tau,\hat{\ell}}$, $\mathbb{E}\left[|x_l|^2\right] = P_l$, and $\mathbb{E}\left[|x_{\hat{\ell}}|^2\right] = P_{\hat{\ell}}$. Moreover, $\{P_l, P_{\hat{\ell}}\}$ are the transmit powers of L_r and L_t users/BSs, and $\{\mathbf{w}_l, \mathbf{w}_{\hat{\ell}}\}$ are the normalized beamforming vectors. Additionally, $\{h_{r,l}, h_{t,\hat{\ell}}\}$ are the path-losses with molecular absorption, $\{h_{p,n,l}, h_{p,\tau,\hat{\ell}}\}$ are the beam misalignment, and $\{h_{f,n,l}, h_{f,\tau,\hat{\ell}}\}$ are the random fog, which can described similar to (3), (6), and (10), respectively.

Therefore, using (49), the received SINR is expressed as

$$\gamma = \frac{h_r^2 \sum_{m=1}^{M} X_m}{\frac{h_t^2}{\text{SIR}} Y + \sum_{l=1}^{L_r} \sum_{n=1}^{K_1} \frac{h_{r,l}^2}{\text{SIR}_l} Y_{n,l} + \sum_{\hat{\ell}=1}^{L_t} \sum_{\tau=1}^{K_2} \frac{h_{t,\hat{\ell}}^2}{\text{SIR}_{\hat{\ell}}} Y_{\tau,\hat{\ell}} + \frac{1}{\text{SNR}}}$$
$$\triangleq \frac{h_r^2 \sum_{m=1}^{M} X_m}{Z + \frac{1}{\text{SNR}}}, \tag{50}$$

where X_m and Y are respectively given in (14) and (15), $Y_{n,l} \triangleq \left| h_{p,n,l} h_{f,n,l} \sum_{i=1}^{N} h_{i,n,l} \sqrt{\delta_i^r} e^{j\theta_i^r} g_{i,l} \right|^2$, $\text{SIR}_l \triangleq \frac{P_s}{P_l}$, $Y_{\tau,\hat{\ell}} \triangleq \left| h_{p,\tau,\hat{\ell}} h_{f,\tau,\hat{\ell}} \sum_{i=1}^{N} h_{i,\tau,\hat{\ell}} \sqrt{\delta_i^t} e^{j\theta_i^t} g_{i,\hat{\ell}} \right|^2$, and $\text{SIR}_{\hat{\ell}} \triangleq \frac{P_s}{P_{\hat{\ell}}}$.

By comparing (13) and (50), it is obvious that in the denominator, the RV Y is replaced with Z. This is because Z takes into account not only the IUI signal power but also the reflected and transmitted ICI signals. Therefore, by using the MGF and CHF of Z instead of those of Y in Lemma 1, Lemma 2, and Lemma 3, the ergodic capacity, outage probability, and SER of the downlink user in the presence of IUI and ICI caused by multiple users/BSs are readily obtained. As a result, the MGF of Z, $\mathcal{M}_Z(-s) = \mathbb{E}\left[e^{-sZ}\right]$, and CHF of Z, $\Phi_Z(\omega) = \mathbb{E}\left[e^{j\omega Z}\right]$, can be respectively expressed as

$$\mathcal{M}_Z(-s) = \mathcal{M}_Y(-s) \prod_{l=1}^{L_r} \left[\mathcal{M}_{Y_l}(-s)\right]^{K_1} \prod_{\hat{\ell}=1}^{L_t} \left[\mathcal{M}_{Y_{\hat{\ell}}}(-s)\right]^{K_2}, \tag{51}$$

$$\Phi_Z(\omega) = \Phi_Y(\omega) \prod_{l=1}^{L_r} \left[\Phi_{Y_l}(\omega)\right]^{K_1} \prod_{\hat{\ell}=1}^{L_t} \left[\Phi_{Y_{\hat{\ell}}}(\omega)\right]^{K_2}, \tag{52}$$

where $\mathcal{M}_Y(-s) = \left(1 + \frac{s h_t^2 \eta_y}{\text{SIR}}\right)^{-\xi_y - 1}$ is given in (28), and $\Phi_Y(\omega) = \left(1 - j\omega \frac{h_t^2 \eta_y}{\text{SIR}}\right)^{-\xi_y - 1}$. Moreover, for brevity, $\mathcal{M}_{Y_l}(-s) = \mathbb{E}\left[e^{-s \frac{h_{r,l}^2}{\text{SIR}_l} Y_{n,l}}\right]$, $\mathcal{M}_{Y_\ell}(-s) = \mathbb{E}\left[e^{-s \frac{h_{t,\ell}^2}{\text{SIR}_\ell} Y_{\tau,\ell}}\right]$, $\Phi_{Y_l}(\omega) = \mathbb{E}\left[e^{j\omega \frac{h_{r,l}^2}{\text{SIR}_l} Y_{n,l}}\right]$, and $\Phi_{Y_\ell}(\omega) = \mathbb{E}\left[e^{j\omega \frac{h_{t,\ell}^2}{\text{SIR}_\ell} Y_{\tau,\ell}}\right]$ are written similar to the MGF and CHF of Y.

IV. Results and Discussion

We provide numerical and computer simulation results to verify the accuracy of the analytical expressions and assess the impacts of various factors on STAR-RIS assisted THz systems, including beam misalignment, random foggy conditions, phase shift quantization errors, reflection/transmission amplitude coefficients of the STAR-RIS elements, IUI and ICI. Moreover, the performance of the system is compared under both ES and MS protocols with that of a classical reflecting-only RIS-assisted HD system. The results are produced using the parameters provided in TABLE III, unless otherwise stated.

Fig. 4 illustrates the ergodic capacity of U1 against SNR for different numbers of transmit antennas and STAR-RIS elements, where both the desired and IUI links suffer from beam misalignment (pointing errors) and moderate foggy weather. As shown in the figure, the analytical and simulation results are identical, which confirms the accuracy of Lemma 1 given in (22). It also compares the capacity performance in the presence of optimal ($\phi^r = 0$) and non-optimal STAR-RIS phase shifts ($\phi^r \neq 0$), which shows the significant impacts of phase shift quantization errors. For example, in the ES protocol, for $M = 2$, $N = 100$, SIR $= 10$ dB and $\delta^t = \delta^r = 0.5$, the capacity achieved with a one-bit phase shift quantizer/two quantization levels ($Q = 2$) is significantly lower compared to that of the optimal phase shifts.

Furthermore, according to (13), increasing the number of transmit antennas improves the SINR, which in turn leads to improvements in the ergodic capacity. In addition, increasing the number of STAR-RIS elements improves both the desired and IUI signal powers. However, the improvement in the desired signal power is much greater than that of the IUI. The reason for this is that the IUI signals are not beamformed

TABLE III Simulation Parameters

Parameter Name	Value
Number of transmit antennas	$M = \{1, 2, 4\}$
Number of receive antennas	$M_r = 2$
Number of STAR-RIS elements	$N = \{10, 20, 30\}$ $N = \{50, 100, 200, 300\}$
STAR-RIS amplitude coefficients	$\delta^t = \delta^r = \{0.5, 1\}$ $\delta^r = \{0.65, 0.75\}$
Carrier frequency	$f = 300$ GHz
Antenna gains	$G_{\text{BS}} = 45$ dBi, $G_t = G_r = 40$ dBi
Speed of light	$c = 3 \times 10^8$ m/sec
Distances	$d_{\text{BS}} = 15$ m, $d_t = d_r = 10$ m
Relative humidity	$\phi_H = 50\%$ [13]
Temperature	$T = 27^o C$ [13]
Atmospheric pressure	$\varrho = 101325$ Pa [12]
Standard deviations of pointing errors displacement	$\sigma_m = \sigma_t = 0.01$ m [9]
Normalized beamwidths	$\frac{w_{d_{\text{BS}}}}{a_r} = 2.5$, $\frac{w_{d_t}}{a_r} = 3$ [9]
Light fog parameters	$k = 2.32$, $\theta = 13.12$ [14]
Moderate fog parameters	$k = 5.49$, $\theta = 12.06$ [14]
Thick fog parameters	$k = 6$, $\theta = 23$ [16]
Dense fog parameters	$k = 36.05$, $\theta = 11.91$ [16]
Complex Gaussian channels	$h_m, h, g \sim \mathcal{CN}(1, 1)$ [13]
Phase shift quantization levels	$Q = \{2, 4, 8\}$
Signal-to-noise ratio	SNR $= \{35, 50\}$ dB
Signal-to-interference ratio	SIR $= \{10, 20, 30\}$ dB
SINR threshold	$\gamma_{th} = \{5, 10\}$ dB
Modulation parameters (QPSK and 16QAM)	$(a, b) = \{(2, 1), (3, \frac{1}{10})\}$ [53]

towards U1, as the transmitting elements of the STAR-RIS are configured to direct the incident signals towards the BS, not U1. As a result, the greater the number of STAR-RIS elements, the higher the ergodic capacity is achieved. For instance, as shown in Fig. 4, in the ES protocol, for the same SNR, $M = 2$ and $Q = 2$, the ergodic capacity exhibits a significant increase by raising N from 100 to 200, and it is further improved by increasing M from 2 to 4, which is consistent with (24).

Fig. 4 also compares the ergodic capacity achieved under the ES and MS protocols, where the number of STAR-RIS elements and amplitude coefficients are set as $\{N = 100, \delta^r = \delta^t = 0.5\}$ and $\{N_r = N_t = N/2, \delta^r = \delta^t = 1\}$ for the ES and MS protocols, respectively. The figure shows that the ES protocol outperforms the MS protocol. This is because, under the MS protocol, while the number of elements randomly transmitting the IUI signals is reduced, the number of elements reflecting the beamformed desired signal is also reduced. As a result, this adversely affects the desired signal power and ergodic capacity. Moreover, as shown in the figure, regardless of the STAR-RIS protocols and system parameters, the ergodic capacity in the high-SNR regime (i.e. SNR > 70 dB) due to IUI signals reaches a limit (capacity ceiling). However, the limit is scaled by various parameters, including the number of antennas, STAR-RIS elements, protocols, and phase shifts; consequently, this observation confirms Remark 1.

Fig. 5 compares the total system capacity of FD (under ES and MS protocols) with the capacity of a reflecting-only RIS-assisted HD downlink system in the presence of moderate foggy weather, beam misalignment and non-optimal phase shifts ($Q = 2$). In this comparison, the numbers of transmit and receive antennas are set as $M = M_r = 2$, SIR $= 10$ dB, and the numbers of STAR-RIS elements and amplitude coefficients are set as $\{N = 100, \delta^r = \delta^t = 0.5\}$ for the

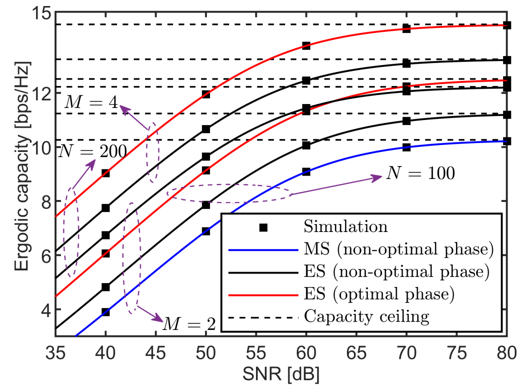

Fig. 4 Ergodic capacity versus SNR for optimal/non-optimal phase shifts and different number of antennas and STAR-RIS elements.

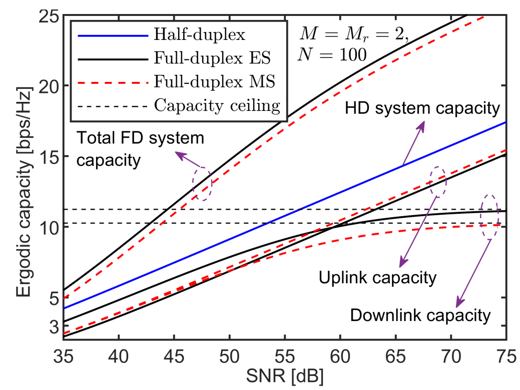

Fig. 5 Comparison of total capacity of STAR-RIS assisted FD system (with ES and MS) and reflecting-only RIS-assisted HD system.

ES protocol, $\{N_r = N_t = N/2, \delta^r = \delta^t = 1\}$ for the MS protocols, and $\{N = 100, \delta^r = 1\}$ for the HD system.

Fig. 5 demonstrates that, regardless of the STAR-RIS operating protocol, the FD system achieves a significantly higher capacity compared to the classical reflecting-only RIS-assisted HD system. This is because, unlike the HD system that allows only U1 to utilize the frequency resources, the FD process enables both U1 and U2 to simultaneously utilize the same frequency resources. Fig. 5 also reveals that while the uplink capacity in the ES protocol is lower compared to that of the MS protocol due to selection errors associated with the coupled phase shifts, the total capacity of the FD system is higher in the ES protocol. Moreover, it is observed that the downlink capacity is higher in the relatively low-SNR regime than that of the uplink, since the downlink user (U1) is not affected by selection errors. In contrast, the uplink capacity is higher in the high-SNR regime, since IUI limits the downlink user's (U1's) capacity in this regime.

Fig. 6 illustrates the impacts of different foggy conditions and beamwidth of the desired links on the ergodic capacity of U1, with $Q = 4$, SIR $= 20$ dB, SNR $= 50$ dB, $M = 4$, and $N = 200$. As a benchmark, the ergodic capacity in the absence of beam misalignment for the desired signal is also provided. It can be clearly seen that, in all types of fog, an increase in the normalized beamwidth, $w_{d_{\text{BS}}}/a_r$, leads to a significant degradation in the ergodic capacity. The reason behind this is that according to (8), higher values of the normalized beamwidth imply that a lower amount of the desired signal power is

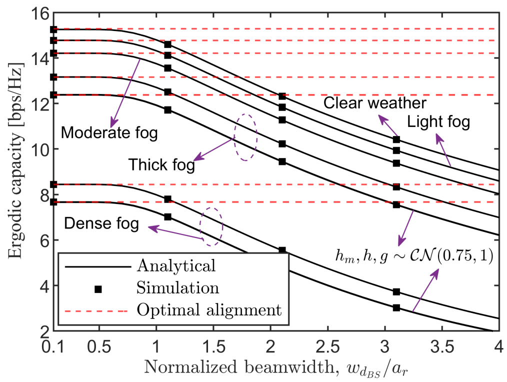

Fig. 6 Impacts of different foggy weather conditions and beamwidth of the desired links on the ergodic capacity.

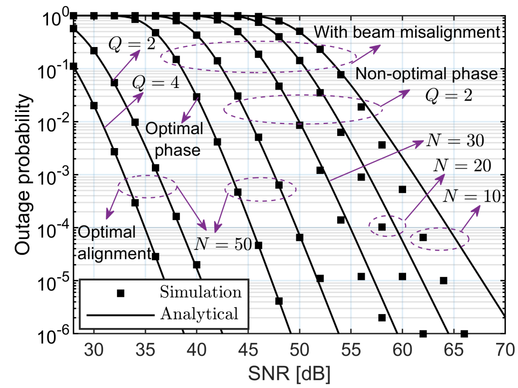

Fig. 7 Impacts of beam misalignment and non-optimal phase shift along with the quantization levels on the outage probability.

collected at U1, which results in significant pointing errors and a reduction in the SINR. Moreover, various foggy conditions may lead to different fading characteristics, and thus for thick fog and dense fog conditions, the capacity is also depicted for $h_m, h, g \sim \mathcal{CN}(0.75, 1)$, illustrating the severe effects of random fog on the capacity performance. Furthermore, the figure indicates that for $w_{d_{\text{BS}}}/a_r \leq 0.5$, the ergodic capacity remains stable and almost identical to that of the perfectly aligned condition. This stability arises because, at values of $w_{d_{\text{BS}}}/a_r \leq 0.5$, the fraction of power collected by U1, as described in (8), becomes $A_m = \left[\text{erf}\left(\sqrt{\frac{\pi}{2}}\frac{a_r}{w_{d_{\text{BS}}}}\right)\right]^2 \approx 1$. Consequently, it implies that the desired signals arrive with very narrow beamwidths, which enables U1 to capture almost all of the desired power.

In order to evaluate the detrimental effects of random fog, the ergodic capacity is compared to a benchmark established under clear weather (non-foggy) condition, as shown in Fig. 6. It is observed that regardless of pointing errors, the deterioration of the ergodic capacity depends on the fog density, i.e. amount of atmospheric water droplets and ice crystals. For instance, for different values of the normalized beamwidth, as the fog density increases (from clear weather to light fog, moderate fog, thick fog and finally dense fog), the ergodic capacity decreases. This is because highly-dense fog particles in the propagation environment result in significant signal attenuation, which adversely affects the ergodic capacity.

Fig. 7 illustrates the outage probability under the ES protocol and thick fog with $M = 2$, $N = \{10, 20, 30, 50\}$, $\gamma_{th} = 5$ dB, and SIR $= 30$ dB. As shown, for a small number of STAR-RIS elements ($N = \{10, 20\}$), the analytical results are less accurate compared to the computer simulation results. However, when increasing N to 30 and 50, their agreement improves significantly, confirming the convergence and accuracy of the Laguerre expansion approximations and Lemma 2 given in (16), (19), and (29)/(30), respectively. Moreover, the outage probability under optimal phase shifts is used as a benchmark to evaluate the impact of phase shift quantization errors. It is shown that non-optimal phase shifts have remarkable impacts on the outage probability, as depicted for $N = 50$ under beam misalignment. This is because, non-optimal phase shifts result in non-optimal beamforming towards U1, leading to attenuation in the desired signal power and adverse effects on the SINR and outage probability.

Fig. 7 also shows that the impacts of phase shift quantization errors are greatly mitigated by increasing the level of quantization. For instance, for $N = 50$ and optimal alignment, non-optimal phase shifts with $Q = 4$ result in a much lower outage probability compared to those with $Q = 2$. However, this improvement comes at the price of increased hardware complexity and cost, as achieving higher precision requires more quantization bits. The outage probability is further assessed by evaluating the impacts of pointing errors or beam misalignment, which are found to have a greater impact than phase shift quantization errors. For example, for $N = 50$, it is shown that in the presence of beam misalignment, an outage probability of 10^{-4} is achieved with optimal and non-optimal phase shifts ($Q = 2$) at SNR values of 46 dB and 50 dB, respectively. However, in the absence of beam misalignment with non-optimal phase shifts ($Q = 2$), the same outage probability is achieved at a much lower SNR of 38 dB, which confirms the catastrophic impacts of beam misalignment.

Fig. 8 compares the outage probability of U1 assisted by a STAR-RIS operating under ES and MS protocols, with that of the reflecting-only RIS-assisted HD system in the presence of beam misalignment, non-optimal phase shifts, and thick fog with $\gamma_{th} =$ SIR $= 10$ dB. In this comparison, the number of STAR-RIS elements and amplitude coefficients are set as $\{N = 50, \delta^r = \delta^t = 0.5\}$ for the ES protocol, $\{N_r = N_t = N/2, \delta^r = \delta^t = 1\}$ for the MS protocol, and $\{N = 50, \delta^r = 1\}$ for the HD system. As shown in the figure, for the same $M = 2$ and $Q = 2$, the ES protocol exhibits better performance than the MS protocol. This is because in the MS protocol, there is a decrease not only in the number of STAR-RIS elements that randomly transmit the IUI signals but also in the elements that reflect the beamformed desired signals. As a result, this has a detrimental effect on the power of the desired signals, leading to a higher outage probability.

Fig. 8 also demonstrates that the reflecting-only RIS-assisted HD downlink system exhibits a lower outage probability, as it is not affected by IUI signals. Nevertheless, by increasing the quantization levels of the STAR-RIS employed for the FD system (e.g. from $Q = 2$ to $Q = 8$), the outage probability of U1 significantly improves in the relatively low-SNR regime (e.g. for SNR ≤ 57 dB), surpassing that of the HD system. This is because higher levels of phase shift quantization lead

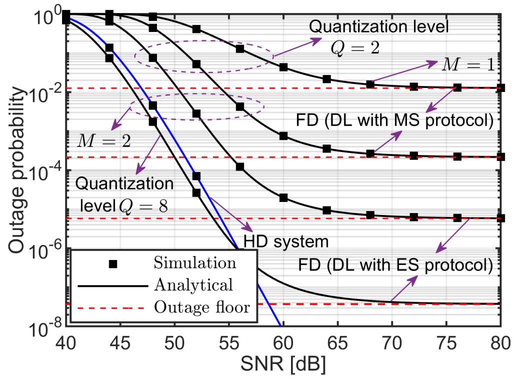

Fig. 8 Outage probability of U1 with STAR-RIS assisted FD system (ES and MS protocols) and reflecting-only RIS-assisted HD system.

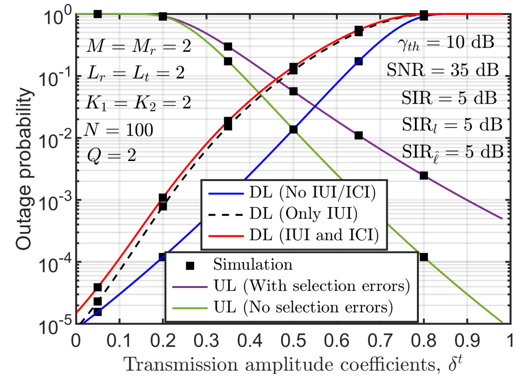

Fig. 9 Impacts of IUI, ICI and STAR-RIS amplitude coefficients on the outage probability of downlink and uplink communications.

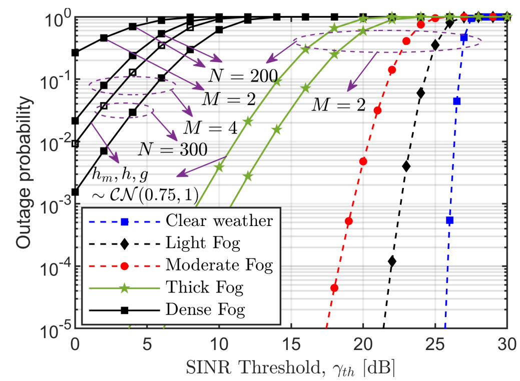

Fig. 10 Impacts of various foggy conditions on the outage probability for different numbers of STAR-RIS elements and transmit antennas.

to accurate and strong beamforming towards U1, resulting in mitigation of IUI signals and improved SINR. Moreover, it should be emphasized that the IUI signals introduce an outage probability limit (outage floor) in the high-SNR regime, which confirms Remark 1. However, it is scaled by quantization levels, number of antennas, and STAR-RIS operating protocols.

Fig. 9 illustrates the outage probability of downlink and uplink communications against the transmission amplitude coefficients of the STAR-RIS in the presence of non-optimal phase shifts, moderate foggy weather, and non-optimal beam alignment, for $M_r = M = 2$, $N = 100$, SIR $= 5$ dB, SNR $= 35$ dB, and $\gamma_{th} = 10$ dB. It also assesses the impacts of ICI signals reflected and transmitted by the STAR-RIS towards U1. In this assessment, the numbers of ICI users/BSs located in the vicinity of the reflection and transmission spaces are set as $L_r = 2$ and $L_t = 2$ respectively, with each having $K_1 = K_2 = 2$ transmit antennas. Additionally, the distances of the interfering users/BSs to the STAR-RIS are assumed to be 35 m, and the rest of the required parameters of ICI users/BSs are set to be the same as those of IUI. By recalling the ES protocol and referring to (13) and (31), it can be stated that an increase in the transmission amplitude coefficients leads to an increase in the IUI signal power. As a result, this leads to considerable deterioration in the SINR and the outage probability of downlink communication, as shown in Fig. 9. In contrast, it improves the outage probability of uplink communication. The is due to fact that the STAR-RIS elements transmit more energy of the incident signals than they reflect.

It should be noted that, in the considered setup, to mitigate the effects of IUI, the downlink user is assumed to be the primary beneficiary for phase shift design. Consequently, when accounting for a practical STAR-RIS, the phase shifts of both reflecting and transmitting elements are coupled, leading to selection errors that greatly impact the outage performance of uplink communication, as shown in Fig. 9. Therefore, to achieve a reliable FD system, optimizing the STAR-RIS amplitude coefficients for uplink and downlink with coupled phase shifts is essential, but it exceeds the scope of this paper. Moreover, Fig. 9 also shows that the effects of ICI signals arising from adjacent cells' users and BSs remain minimal and negligible for varying values of δ^t. This outcome is primarily attributed to the considerable inter-cell distances, STAR-RIS phase shifts, and practical limitations of THz communications.

Figure 10 shows the outage probability of U1 against the SINR threshold under various foggy conditions and ES protocol for $M = \{2, 4\}$, $N = \{200, 300\}$, $\frac{w_{d_{\text{BS}}}}{a_r} = 3$, $\frac{w_{d_t}}{a_r} = 6$, SNR $= 50$ dB, SIR $= 20$ dB, and $Q = 8$. It also shows the outage probability under clear weather condition to evaluate the impacts of fog on the system reliability. As shown in the figure, as the SINR threshold increases, the outage probability increases. Moreover, as the fog density increases, the outage probability worsens significantly, causing severe unreliability in the communication. For example, for $(M, N) = (2, 200)$, the minimum threshold values where the outage probability becomes $P_o = 1$ and the communication cannot be established, are 28.5 dB, 27 dB, 26 dB, 24 dB, and 9 dB for clear weather, light fog, moderate fog, thick fog, and dense fog, respectively. However, increasing the number of transmit antennas and STAR-RIS elements, mitigates the impacts of fog. For example, under dense fog, by increasing M from 2 to 4, the threshold where $P_o = 1$ is increased from 9 dB to 12 dB, and it is further enhanced to 14 dB by increasing N from 200 to 300. This improvement is due to the increase in desired signal power resulting from more transmit antennas and STAR-RIS elements. Additionally, considering the effects of random fog on the fading channels, the outage probability is examined under thick and dense fog conditions for $h_m, h, g \sim \mathcal{CN}(0.75, 1)$, which greatly deteriorates the system reliability compared to that of $h_m, h, g \sim \mathcal{CN}(1, 1)$.

Fig. 11 illustrates the combined effects of beam misalignment, random fog, and phase shift quantization errors on the SER of U1 under ES protocol and QPSK modulation with $M = 2$, $N = \{10, 20, 30, 50\}$ and SIR $= 30$ dB. It is shown that for a small number of STAR-RIS elements ($N = \{10, 20\}$), the analytical results are less accurate compared to the exact simulation results. However, as N is increased to 30 and 50, their agreement improves significantly. This confirms the convergence and accuracy of the Laguerre expansion approximations and Lemma 3 as given in (16), (19), and (36)/(38), respectively. The comparison between the SER achieved under optimal and non-optimal phase shifts ($Q = 2$) highlights the notable impact of quantization errors, as exemplified for $N = 50$.

Fig. 11 also provides a comparison between the SER achieved under optimal clear weather and thick foggy weather, revealing the significant effects of random fog on the SER. The presence of concentrated fog particles in the propagation environment results in notable signal attenuation, adversely impacting both the desired and IUI signals. However, the impact is more dominant on the beam-formed desired signals, leading to a greater adverse impact on the SINR and SER. Finally, the SER performance under beam misalignment and perfectly aligned desired links is compared. The results indicate that beam misalignment has a significantly greater impact than random fog and phase shift quantization errors, as exemplified for $N = 50$. Therefore, to achieve better performance, the antennas along with the STAR-RIS need to be properly aligned. Since different foggy conditions may lead to different fading characteristics, the SER performance under thick fog, optimal alignment and $N = 50$ is also provided for $h_m, h, g \sim \mathcal{CN}(0.75, 1)$. The obtained results demonstrate the catastrophic impacts of random fog on the SER performance.

Fig. 12 compares the SER performance of U1 assisted by a STAR-RIS operating under ES and MS protocols with that of the reflecting-only RIS-assisted HD system, considering beam misalignment, non-optimal phase shifts ($Q = 2$), thick fog, $M = 2$, SIR $= 10$ dB, and 16QAM modulation. In this comparison, the system parameters are set as follows: for the ES protocol $N = 50$, $\delta^r = \{0.5, 0.65, 0.75\}$ and $\delta^t = 1 - \delta^r$; for the MS protocol $\{N_r = N_t = N/2, \delta^r = \delta^t = 1\}$; and for the HD system $\{N = 50, \delta^r = 1\}$. As shown, the ES protocol demonstrates superior SER performance compared to the MS protocol. This situation arises because, in the MS protocol, there is a decrease not only in the number of STAR-RIS elements that randomly transmit the IUI signals but also in the elements that reflect the beamformed desired signals.

Moreover, in both ES and MS protocols, the IUI signals pose a limit on the SER in the high-SNR regime, which scales with increasing the reflection amplitude coefficients and quantization levels, validating Remark 1. In addition, Fig. 12 shows that the reflecting-only RIS-assisted HD system provides a lower SER compared to the FD STAR-RIS assisted system due to the absence of IUI signals. However, by increasing the phase shift quantization levels of the STAR-RIS operating under the ES protocol (e.g. from $Q = 2$ to $Q = 8$), a significant improvement is observed in the SER performance of U1. This improvement enables it to outperform the HD system in the relatively low-SNR regime (SNR ≤ 62 dB), while it remains restricted in the high-SNR regime due to IUI signals.

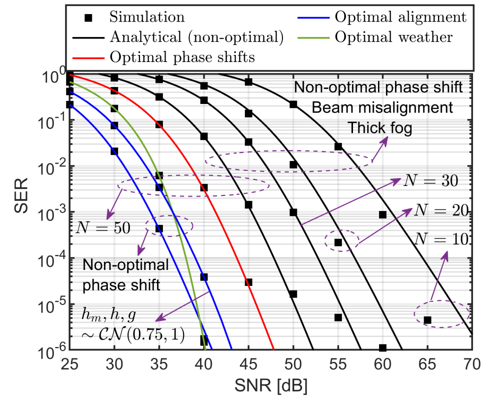

Fig. 11 Effects of random fog, STAR-RIS phase shift errors and beam misalignment on the SER for QPSK and different values of N.

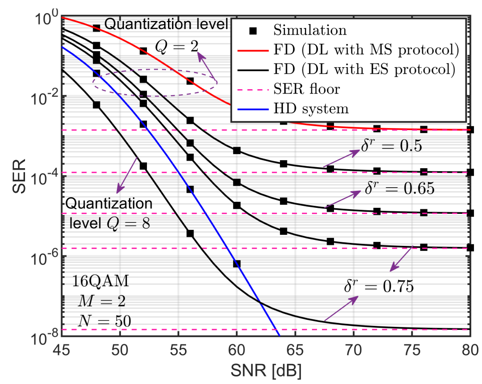

Fig. 12 SER of a STAR-RIS assisted FD system under ES and MS protocols and reflecting-only RIS-assisted HD system for 16QAM.

V. Conclusion

This paper focused on the performance of a STAR-RIS assisted THz system in the presence of interference, and presented new expressions for the ergodic capacity, outage probability and SER. It also accurately approximated the statistical distributions of the desired and interference signals' power using the Laguerre expansion. It was shown that the adverse effects of beam misalignment and random fog are more severe compared to interference and phase shift quantization errors under both ES and MS protocols. Nonetheless, they can be reduced by increasing the number of antennas and STAR-RIS elements. It was also shown that the ES protocol outperforms the MS protocol, and under both protocols, the system performance reaches a limit in the high-SNR regime due to IUI. Moreover, it was shown that the effects of interference stemming from multiple users and BSs situated in neighboring cells are negligible. The total system capacity of the FD STAR-RIS assisted system significantly outperforms that of the reflecting-only RIS-assisted HD downlink system. Furthermore, by increasing the quantization levels, the outage probability and SER of the STAR-RIS also outperform those of the HD system. Additionally, selection errors resulting from coupled phase shifts notably affect the uplink performance, which can be reduced by increasing the transmission amplitude coefficients, but this raises IUI signal power and lowers downlink performance. Therefore, this gives rise to an optimization problem of enhancing users' performance while mitigating interference, taking into account the coupled phase shifts.

Appendix A

In order to calculate μ_x and σ_x^2 given in (17) and (18), we first need to calculate $\mathbb{E}[\lambda_m]$, $\mathbb{V}[\lambda_m]$, and the moments of $h_{p,m}$ and $h_{f,m}$, i.e. $\mathbb{E}\left[h_{p,m}^\ell\right]$ and $\mathbb{E}\left[h_{f,m}^\ell\right]$. Let's rewrite $\lambda_m \triangleq \lambda_R^2 + \lambda_I^2$ with $\lambda_R \triangleq \sum_{i=1}^N |h_{m,i}|\,|g_i|\,\sqrt{\delta_i^r}\cos\phi_i^r$ and $\lambda_I \triangleq \sum_{i=1}^N |h_{m,i}|\,|g_i|\,\sqrt{\delta_i^r}\sin\phi_i^r$. Moreover, $h_{m,i} \sim \mathcal{CN}(\mu_{h_{m,i}}, \sigma_{h_{m,i}}^2)$ and $g_i \sim \mathcal{CN}(\mu_{g_i}, \sigma_{g_i}^2)$ are assumed to be non-zero mean complex Gaussian RVs, where their amplitudes follow Rician distribution. As mentioned in Section II-A, when the Euclidean distance between two adjacent RIS elements is greater than half of the carrier wavelength, the assumption of IID channels across the elements can be adopted [8], [41]. Therefore, for the sake of simplicity, we omit the subscript i and write $h_{m,i} \triangleq h_m \sim \mathcal{CN}(\mu_{h_m}, \sigma_{h_m}^2)$, $g_i \triangleq g \sim \mathcal{CN}(\mu_g, \sigma_g^2)$, $\delta_i^r \triangleq \delta^r$, and $\phi_i^r \triangleq \phi^r$. Thus, using [13, Eq. (13)], the mean and variance of λ_m are respectively expressed as

$$\begin{aligned}\mathbb{E}[\lambda_m] &= \mathbb{E}\left[\lambda_R^2\right] + \mathbb{E}\left[\lambda_I^2\right] \\ &= N\delta^r\left[\bar{\mu}_1\bar{\mu}_2 + (N-1)\mu_1^2\mu_2^2\mathcal{F}_1^2\right],\end{aligned} \tag{53}$$

$$\begin{aligned}\mathbb{V}[\lambda_m] &= \mathbb{V}\left[\lambda_R^2\right] + \mathbb{V}\left[\lambda_I^2\right] \\ &= (N\delta^r)^2\left[\bar{\mu}_1^2\bar{\mu}_2^2\left(1+\mathcal{F}_2+0.5\mathcal{F}_2^2\right) + (2N-2)\,\bar{\mu}_1\bar{\mu}_2\right. \\ &\quad \left.\times\mu_1^2\mu_2^2\mathcal{F}_1^2\left(1+\mathcal{F}_2\right) - (4N-2)\,\mu_1^4\mu_2^4\mathcal{F}_1^4\right],\end{aligned} \tag{54}$$

where $\bar{\mu}_1 = \mathbb{E}\left[|h_m|^2\right]$, $\bar{\mu}_2 = \mathbb{E}\left[|g|^2\right]$, $\mu_1 = \mathbb{E}[|h_m|]$, $\mu_2 = \mathbb{E}[|g|]$, $\mathcal{F}_1 = \frac{\sin(\pi/Q)}{\pi/Q}$ and $\mathcal{F}_2 = \frac{\sin(2\pi/Q)}{2\pi/Q}$ [13]. Moreover, the ℓ-th moments of $|h_m|$ and $|g|$ are written as $\mathbb{E}\left[|h_m|^\ell\right] = \sigma_{h_m}^\ell\Gamma\left(1+\ell/2\right)L_{\ell/2}\left(-\mu_{h_m}^2/\sigma_{h_m}^2\right)$ and $\mathbb{E}\left[|g|^\ell\right] = \sigma_g^\ell\Gamma\left(1+\ell/2\right)L_{\ell/2}\left(-\mu_g^2/\sigma_g^2\right)$ [56].

The ℓ-th moment of $h_{p,m}$ is written as $\mathbb{E}\left[h_{p,m}^\ell\right] = \frac{\xi_m}{\xi_m+\ell}A_m^\ell$ [9, Eq. (A-2)]. Moreover, using (10), the ℓ-th moment of $h_{f,m}$ is written as $\mathbb{E}\left[h_{f,m}^\ell\right] = \mathbb{E}\left[e^{-\ell\frac{\beta(d_{\rm BS}+d_r)}{4343}}\right]$. Since β is a gamma RV, by exploiting its MGF given in [56, TABLE 2.3-3], we can write that $\mathbb{E}\left[h_{f,m}^\ell\right] = \left(1+\frac{\ell\theta(d_{\rm BS}+d_r)}{4343}\right)^{-k}$, where the values of θ and k for different types of foggy conditions are given in Section II-D. Finally, by substituting the corresponding mean, variance and statistical moments terms into (17) and (18), the mean and variance of X_m are obtained. ■

Appendix B

In order to calculate μ_y and σ_y^2, we need to derive $\mathbb{E}\left[|\lambda|^2\right]$, $\mathbb{V}\left[|\lambda|^2\right]$, $\mathbb{E}\left[h_{p,t}^\ell\right]$ and $\mathbb{E}\left[h_{f,t}^\ell\right]$. It can be rewritten that $\lambda \triangleq \sum_{i=1}^N h_i\sqrt{\delta_i^t}e^{j\theta_i^t}g_i$, where $h_i \sim \mathcal{CN}(\mu_{h_i}, \sigma_{h_i}^2)$ and $g_i \sim \mathcal{CN}(\mu_{g_i}, \sigma_{g_i}^2)$ are non-zero mean complex Gaussian RVs, and $\theta_i^t \in [0, 2\pi)\ \forall i = 1, \ldots, N$ are uniformly distributed RVs [13], [43]. Moreover, for the sake of simplicity, similar to Appendix A, we adopt the assumption of IID channels across the STAR-RIS elements. As a result, we can omit the subscript i and represent h_i as $h \sim \mathcal{CN}(\mu_h, \sigma_h^2)$, g_i as $g \sim \mathcal{CN}(\mu_g, \sigma_g^2)$, θ_i^t as θ^t, and δ_i^t as δ^t. Therefore, according to [43, Proposition 2], for a sufficiently large number of STAR-RIS elements, λ converges to a complex Gaussian RV, i.e. $\lambda \sim \mathcal{CN}\left(\mu_\lambda, \sigma_\lambda^2\right)$.

On the other hand, since $\theta^t \in [0, 2\pi)$, it can be written that $\mathbb{E}[\cos\theta^t] = \mathbb{E}[\sin\theta^t] = 0$, $\mathbb{E}\left[\cos^2\theta^t\right] = 1/2 + \mathbb{E}[\cos 2\theta^t]/2 = 1/2$ and $\mathbb{E}\left[\sin^2\theta^t\right] = 1/2 - \mathbb{E}[\cos 2\theta^t]/2 = 1/2$ [42], [43]. Therefore, $\mu_\lambda = 0$ and $\sigma_\lambda^2 = N\delta^t\left(\sigma_h^2+\mu_h^2\right)\left(\sigma_g^2+\mu_g^2\right)$. Furthermore, $|\lambda|^2$ follows exponential distribution with $\mathbb{E}\left[|\lambda|^2\right] = \sigma_\lambda^2$ and $\mathbb{V}\left[|\lambda|^2\right] = \sigma_\lambda^4$. In addition, the ℓ-th moments of $h_{f,t}$ and $h_{p,t}$ are respectively written as $\mathbb{E}\left[h_{f,t}^\ell\right] = \left(1+\frac{\ell\theta(d_t+d_r)}{4343}\right)^{-k}$ and $\mathbb{E}\left[h_{p,t}^\ell\right] = \frac{\xi_t}{\xi_t+\ell}A_t^\ell$ [9, Eq. (A-2)]. Finally, by substituting the corresponding mean, variance and moments terms into (20) and (21), the mean and variance of Y are obtained. ■

References

[1] Z. Chen, X. Ma, C. Han, and Q. Wen, "Towards intelligent reflecting surface empowered 6G terahertz communications: A survey," *China Commun.*, vol. 18, no. 5, pp. 93–119, May 2021.

[2] H. Do, S. Cho, J. Park, H.-J. Song, N. Lee, and A. Lozano, "Terahertz line-of-sight MIMO communication: Theory and practical challenges," *IEEE Commun. Mag.*, vol. 59, no. 3, pp. 104–109, Mar. 2021.

[3] C. Han, Y. Wang, Y. Li, Y. Chen, N. A. Abbasi, T. Kürner, and A. F. Molisch, "Terahertz wireless channels: A holistic survey on measurement, modeling, and analysis," *IEEE Commun. Surveys Tuts.*, vol. 24, no. 3, pp. 1670–1707, 3rd Quart. 2022.

[4] G. Pan, J. Ye, J. An, and M.-S. Alouini, "Full-duplex enabled intelligent reflecting surface systems: Opportunities and challenges," *IEEE Wireless Commun.*, vol. 28, no. 3, pp. 122–129, Jun. 2021.

[5] T. N. Nguyen, N. N. Thang, B. C. Nguyen, T. M. Hoang, and P. T. Tran, "Intelligent-reflecting-surface-aided bidirectional full-duplex communication system with imperfect self-interference cancellation and hardware impairments," *IEEE Syst. J.*, vol. 17, no. 1, pp. 1352–1362, Mar. 2023.

[6] P. K. Sharma, N. Sharma, S. Dhok, and A. Singh, "RIS-assisted FD short packet communication with non-linear EH," *IEEE Commun. Lett.*, vol. 27, no. 2, pp. 522–526, Feb. 2023.

[7] B. Lu, R. Wang, and Y. Liu, "Outage probability of intelligent reflecting surface assisted full duplex two-way communications," *IEEE Commun. Lett.*, vol. 26, no. 2, pp. 286–290, Feb. 2022.

[8] S. Dhok and P. K. Sharma, "Infinite and finite block-length FD transmissions with spatially-correlated RIS channels," *IEEE Trans. Wireless Commun.*, vol. 22, no. 2, pp. 1060–1071, Feb. 2023.

[9] H. Du, J. Zhang, K. Guan, D. Niyato, H. Jiao, Z. Wang, and T. Kurner, "Performance and optimization of reconfigurable intelligent surface aided THz communications," *IEEE Trans. Commun.*, vol. 70, no. 5, pp. 3575–3593, May 2022.

[10] K. Tekbiyik, G. K. Kurt, A. R. Ektı, and H. Yanikomeroglu, "Reconfigurable intelligent surfaces empowered THz communication in LEO satellite networks," *IEEE Access*, vol. 10, pp. 121 957–121 969, Nov. 2022.

[11] C. Huang, Z. Yang, G. C. Alexandropoulos, K. Xiong, L. Wei, C. Yuen, Z. Zhang, and M. Debbah, "Multi-hop RIS-empowered terahertz communications: A DRL-based hybrid beamforming design," *IEEE J. Select. Areas Commun.*, vol. 39, no. 6, pp. 1663–1677, Jun. 2021.

[12] A.-A. A. Boulogeorgos, E. N. Papasotiriou, and A. Alexiou, "Analytical performance assessment of THz wireless systems," *IEEE Access*, vol. 7, pp. 11 436–11 453, Jan. 2019.

[13] A. M. Tota Khel and K. A. Hamdi, "Secrecy capacity of IRS-assisted terahertz wireless communications with pointing errors," *IEEE Commun. Lett.*, vol. 27, no. 4, pp. 1090–1094, Apr. 2023.

[14] M. A. Esmail, H. Fathallah, and M.-S. Alouini, "On the performance of optical wireless links over random foggy channels," *IEEE Access*, vol. 5, pp. 2894–2903, Feb. 2017.

[15] K. Su, L. Moeller, R. B. Barat, and J. F. Federici, "Experimental comparison of performance degradation from terahertz and infrared wireless links in fog," *JOSA A*, vol. 29, no. 2, pp. 179–184, Feb. 2012.

[16] O. S. Badarneh, "Performance analysis of terahertz communications in random fog conditions with misalignment," *IEEE Wireless Commun. Lett.*, vol. 11, no. 5, pp. 962–966, May 2022.

[17] A.-A. A. Boulogeorgos, J. M. Riera, and A. Alexiou, "On the joint effect of rain and beam misalignment in terahertz wireless systems," *IEEE Access*, vol. 10, pp. 58 997–59 012, Jun. 2022.

[18] O. S. Badarneh, "Joint impact of fog conditions and antenna misalignment on outage and bit error rate in terahertz communications," in *Proc. Int. Conf. Electr., Comput., Commun. Mechatronics Eng. (ICECCME)*, Nov. 2022, pp. 1–6.

[19] X. Mu, Y. Liu, L. Guo, J. Lin, and R. Schober, "Simultaneously transmitting and reflecting (STAR) RIS aided wireless communications," *IEEE Trans. Wireless Commun.*, vol. 21, no. 5, pp. 3083–3098, May 2022.

[20] V. K. Chapala and S. M. Zafaruddin, "Exact analysis of RIS-aided THz wireless systems over $\alpha-\mu$ fading with pointing errors," *IEEE Commun. Lett.*, vol. 25, no. 11, pp. 3508–3512, Nov. 2021.

[21] A.-A. A. Boulogeorgos, N. D. Chatzidiamantis, H. G. Sandalidis, A. Alexiou, and M. D. Renzo, "Cascaded composite turbulence and misalignment: Statistical characterization and applications to reconfigurable intelligent surface-empowered wireless systems," *IEEE Trans. Veh. Technol.*, vol. 71, no. 4, pp. 3821–3836, Apr. 2022.

[22] A. Papazafeiropoulos, P. Kourtessis, and I. Krikidis, "STAR-RIS assisted full-duplex systems: Impact of correlation and maximization," *IEEE Commun. Lett.*, vol. 26, no. 12, pp. 3004–3008, Dec. 2022.

[23] Y. Zhang, B. Di, H. Zhang, Z. Han, H. V. Poor, and L. Song, "Meta-wall: Intelligent omni-surfaces aided multi-cell MIMO communications," *IEEE Trans. Wireless Commun.*, vol. 21, no. 9, pp. 7026–7039, Sep. 2022.

[24] G. Zhou, C. Pan, H. Ren, K. Wang, and A. Nallanathan, "Intelligent reflecting surface aided multigroup multicast MISO communication systems," *IEEE Trans. Signal Processing*, vol. 68, pp. 3236–3251, Apr. 2020.

[25] M. A. ElMossallamy, K. G. Seddik, W. Chen, L. Wang, G. Y. Li, and Z. Han, "RIS optimization on the complex circle manifold for interference mitigation in interference channels," *IEEE Trans. Veh. Technol.*, vol. 70, no. 6, pp. 6184–6189, Jun. 2021.

[26] P. P. Perera, V. G. Warnasooriya, D. Kudathanthirige, and H. A. Suraweera, "Sum rate maximization in STAR-RIS assisted full-duplex communication systems," in *Proc. IEEE Int. Conf. Commun. (ICC)*, May 2022, pp. 3281–3286.

[27] Y. Wang, P. Guan, H. Yu, and Y. Zhao, "Transmit power optimization of simultaneous transmission and reflection RIS assisted full-duplex communications," *IEEE Access*, vol. 10, pp. 61 192–61 200, May 2022.

[28] M. R. Kavianinia, M. J. Emadi, and M. A. Sedaghat, "On resource allocation of STAR-RIS assisted full-duplex systems," *TechRxiv preprint, arXiv:2209.08591*, May 2023.

[29] S. Fang, G. Chen, C. Huang, Y. Gao, Y. Li, K.-K. Wong, and J. A. Chambers, "Weighted sum rate enhancement by using dual-side IOS-assisted full-duplex for multi-user MIMO systems," *TechRxiv preprint, arXiv:2306.17561*, Jun. 2023.

[30] J. Xu, X. Mu, J. T. Zhou, and Y. Liu, "Simultaneously transmitting and reflecting (STAR)-RISs: Are they applicable to dual-sided incidence?" *IEEE Wireless Commun. Lett.*, vol. 12, no. 1, pp. 129–133, Jan. 2023.

[31] J. Xu, J. Zuo, J. T. Zhou, and Y. Liu, "Active simultaneously transmitting and reflecting (STAR)-RISs: Modelling and analysis," *IEEE Commun. Lett.*, pp. 1–1, early access, Jun. 2023.

[32] Y. Liu, J. Xu, Z. Wang, X. Mu, J. Zhang, and P. Zhang, "Simultaneously transmitting and reflecting (STAR) RIS for 6G: Fundamentals, recent advances, and future directions," *TechRxiv preprint, arXiv:2304.14180*, Apr. 2023.

[33] A. Huang, X. Mu, and L. Guo, "STAR-RIS assisted downlink active and uplink backscatter communications with NOMA," *IEEE Trans. Veh. Technol.*, pp. 1–15, early access, Jun. 2023.

[34] K. Xie, G. Cai, G. Kaddoum, and J. He, "Performance analysis and resource allocation of STAR-RIS aided wireless-powered NOMA system," *IEEE Trans. Commun.*, pp. 1–1, early access, Jul. 2023.

[35] R. Zhong, Y. Liu, X. Mu, Y. Chen, X. Wang, and L. Hanzo, "Hybrid reinforcement learning for STAR-RISs: A coupled phase-shift model based beamformer," *IEEE J. Select. Areas Commun.*, vol. 40, no. 9, pp. 2556–2569, Sep. 2022.

[36] S. Yang, J. Zhang, W. Xia, H. Gao, and H. Zhu, "Joint power and discrete amplitude allocation for STAR-RIS-aided NOMA system," *IEEE Trans. Veh. Technol.*, vol. 71, no. 12, pp. 13 382–13 386, Dec. 2022.

[37] Z. Sun and Y. Jing, "On the performance of multi-antenna IRS-assisted NOMA networks with continuous and discrete IRS phase shifting," *IEEE Trans. Wireless Commun.*, vol. 21, no. 5, pp. 3012–3023, May 2022.

[38] W. Shi, J. Xu, W. Xu, M. D. Renzo, and C. Zhao, "Secure outage analysis of RIS-assisted communications with discrete phase control," *IEEE Trans. Veh. Technol.*, vol. 72, no. 4, pp. 5435–5440, Apr. 2023.

[39] H. Zhang, L. Zhang, and X. Yu, "Terahertz band: Lighting up next-generation wireless communications," *China Commun.*, vol. 18, no. 5, pp. 153–174, May 2021.

[40] I. S. Gradshteyn and I. M. Ryzhik, *Table of Integrals, Series, and Products*, 8th ed. Oxford, UK: Academic Press: Elsevier, 2014.

[41] S. Dhok and P. K. Sharma, "Rate-splitting multiple access with STAR RIS over spatially-correlated channels," *IEEE Trans. Commun.*, vol. 70, no. 10, pp. 6410–6424, Oct. 2022.

[42] A. M. Tota Khel and K. A. Hamdi, "Effects of hardware impairments on IRS-enabled MISO wireless communication systems," *IEEE Commun. Lett.*, vol. 26, no. 2, pp. 259–263, Feb. 2022.

[43] J. Lyu and R. Zhang, "Hybrid active/passive wireless network aided by intelligent reflecting surface: System modeling and performance analysis," *IEEE Trans. Wireless Commun.*, vol. 20, no. 11, pp. 7196–7212, Nov. 2021.

[44] A. M. Tota Khel and K. A. Hamdi, "Performance analysis of IRS-assisted full-duplex wireless communication systems with interference," *IEEE Commun. Lett.*, vol. 26, no. 9, pp. 2027–2031, Sep. 2022.

[45] C. C. Chai and T. T. Tjhung, "Unified Laguerre polynomial-series-based distribution of small-scale fading envelopes," *IEEE Trans. Veh. Technol.*, vol. 58, no. 8, pp. 3988–3999, Oct. 2009.

[46] A. Abdi, H. Hashemi, and S. Nader-Esfahani, "On the PDF of the sum of random vectors," *IEEE Trans. Commun.*, vol. 48, no. 1, pp. 7–12, Jan. 2000.

[47] S. Primak, V. Kontorovich, and V. Lyandres, *Stochastic Methods and Their Applications to Communications: Stochastic Differential Equations Approach*. Chichester, U.K.: Wiley, 2004.

[48] M. Abramowitz and I. A. Stegun, *Handbook of Mathematical Functions with Formulas, Graphs, and Mathematical Tables*, 10th ed. New York, NY, USA: Dover, 1972.

[49] K. A. Hamdi, "A useful lemma for capacity analysis of fading interference channels," *IEEE Trans. Commun.*, vol. 58, no. 2, pp. 411–416, Feb. 2010.

[50] P. Billingsley, *Probability and Measures*, 3rd ed. New York, USA: John Wiley & Sons, Inc., 1995.

[51] X. Gan, C. Zhong, Y. Zhu, and Z. Zhong, "User selection in reconfigurable intelligent surface assisted communication systems," *IEEE Commun. Lett.*, vol. 25, no. 4, pp. 1353–1357, Apr. 2021.

[52] A. Nuttall, "Alternate forms for numerical evaluation of cumulative probability distributions directly from characteristic functions," *Proc. IEEE*, vol. 58, no. 11, pp. 1872–1873, Nov. 1970.

[53] A. Goldsmith, *Wireless Communications*. Cambridge, UK: Cambridge Univ. Press, 2005.

[54] K. A. Hamdi, "Some notes on the Fourier transform methods for error-rate analysis of equal-gain combining," *IEEE Trans. Commun.*, vol. 58, no. 12, pp. 3364–3368, Dec. 2010.

[55] E. W. Ng and M. Geller, "A table of integrals of the error functions," *J. Res. Nat. Bureau Stand. B Math. Sci.*, vol. 73B, no. 1, pp. 1–20, Jan.-Mar. 1969.

[56] J. G. Proakis and M. Salehi, *Digital Communications*, 5th ed. New York, NY, USA: McGraw-Hill, 2008.

Ahmad Massud Tota Khel received the B.Sc. degree in electrical and electronics engineering from Istanbul University, Istanbul, Turkey, and the M.Sc. degree (with Distinction) in telecommunications systems from Aston University, Birmingham, U.K. He is currently pursuing the Ph.D. degree in electrical and electronic engineering with The University of Manchester, Manchester, U.K. His research interests include design and analysis of wireless communication networks, reconfigurable intelligent surfaces, physical layer security, millimeter wave and terahertz communications, NOMA, and IoT systems.

Khairi Ashour Hamdi (Senior Member, IEEE) received the B.Sc. degree in electrical engineering from Alfateh University, Tripoli, Libya, in 1981, the M.Sc. degree (Hons.) from the Technical University of Budapest, Budapest, Hungary, in 1988, and the Ph.D. degree in telecommunication engineering from the Hungarian Academy of Sciences, Budapest, in 1993. Previously, he held research and academic posts with the Department of Computer Science, The University of Manchester, and the Department of Electronic Systems Engineering, University of Essex. He was a BT Research Fellow, in Summer 2002, and was a Visiting Assistant Professor with Stanford University, during the academic year 2007–2008. He is currently a Senior Lecturer with The University of Manchester. His current research interests include modeling and performance analysis of wireless communication systems and networks.